NeuroImage 195 (2019) 113–127

Contents lists available at ScienceDirect

NeuroImage

journal homepage: www.elsevier.com/locate/neuroimage

Interhemispheric functional connectivity in the zebra finch brain, absent the corpus callosum in normal ontogeny

Elliot A. Layden [a,*], Kathryn E. Schertz [a], Sarah E. London [a,b,c,1], Marc G. Berman [a,b,1]

[a] Department of Psychology, The University of Chicago, Chicago, IL, 60637, USA
[b] Grossman Institute for Neuroscience, Quantitative Biology and Human Behavior, The University of Chicago, Chicago, IL, 60637, USA
[c] The Institute for Mind and Biology, The University of Chicago, Chicago, IL, 60637, USA

ARTICLE INFO

Keywords:
Corpus callosum
Homotopic functional connectivity
Interhemispheric coordination
Resting-state fMRI
Zebra finch

ABSTRACT

Bilaterally symmetric intrinsic brain activity (homotopic functional connectivity; FC) is a fundamental feature of the mammalian brain's functional architecture. In mammals, homotopic FC is primarily mediated by the corpus callosum (CC), a large interhemispheric white matter tract thought to balance the bilateral coordination and hemispheric specialization critical for many complex brain functions, including human language. The CC first emerged with the Eutherian (placental) mammals ~160 MYA and is not found among other vertebrates. Despite this, other vertebrates also exhibit complex brain functions requiring hemispheric specialization and coordination. For example, the zebra finch (*Taeniopygia guttata*) songbird learns to sing from tutors much as humans acquire speech and must balance hemispheric specialization and coordination to successfully learn and produce song. We therefore tested whether the zebra finch also exhibits homotopic FC, despite lacking the CC. Resting-state fMRI analyses demonstrated widespread homotopic FC throughout the zebra finch brain across development, including within a network required for learned song that lacks direct interhemispheric structural connectivity. The presence of homotopic FC in a non-Eutherian suggests that ancestral pathways, potentially including indirect connectivity via the anterior commissure, are sufficient for maintaining a homotopic functional architecture, an insight with broad implications for understanding interhemispheric coordination across phylogeny.

1. Introduction

Bilaterally symmetric neural activity is among the most striking characteristics of the Eutherian (i.e., placental) mammalian brain's intrinsic functional architecture. This pattern is consistently observed both in humans (Stark et al., 2008; Zuo et al., 2010; Zhang et al., 2014; Shen et al., 2015) and in other mammalian species such as macaques (Vincent et al., 2007; Shen et al., 2015) and rodents (Pan et al., 2011; Matsui et al., 2016). Symmetric brain activity is typically studied by examining temporal correlations (i.e., functional connectivity; FC) embedded within intrinsic (i.e., spontaneous) infra-slow brain activity (<0.1 Hz), conveniently recorded as blood-oxygen-level-dependent (BOLD) signals from resting-state fMRI (rs-fMRI; Biswal et al., 1995, 2010; Mitra et al., 2018). However, consistent results are also obtained using other methods, such as wide-field calcium imaging (Matsui et al., 2016) and local field potentials (Pan et al., 2011). FC between geometrically corresponding, bilateral brain regions is termed homotopic FC (Stark et al., 2008; Zuo et al., 2010; Zhang et al., 2014; Shen et al., 2015). Homotopic FC is: 1) generally much stronger than either ipsilateral or asymmetric interhemispheric (i.e., heterotopic) FC (Stark et al., 2008; Zhang et al., 2014; Shen et al., 2015), 2) more stable across various task and non-task settings than ipsilateral or heterotopic FC (Mišić et al., 2014; Shen et al., 2015), and 3) important for shaping whole-brain network dynamics (Zhang et al., 2014). Homotopic FC also appears to be clinically relevant, with reductions in homotopic FC implicated in diverse human neuropsychiatric (Kelly et al., 2011; Zhang et al., 2014) and neurodegenerative (Zhou et al., 2013) disorders.

FC is only moderately linked to structural connectivity (SC), such as white matter projections ($r \approx 0.50$; Honey et al., 2009), and FC is also capable of arising from functional interactions traversing indirect polysynaptic SC pathways (Vincent et al., 2007; Honey et al., 2009; Lu et al., 2011). Nonetheless, substantial evidence indicates that the direct

* Corresponding author. The Environmental Neuroscience Lab (ENL), 5848 S University Ave, Green Hall 415, Chicago, IL, 60637, USA.
E-mail address: elayden@uchicago.edu (E.A. Layden).
[1] These authors contributed equally to this work.

https://doi.org/10.1016/j.neuroimage.2019.03.064
Received 13 December 2018; Received in revised form 19 March 2019; Accepted 27 March 2019
Available online 30 March 2019

homotopic SC of the corpus callosum (CC; Jarbo et al., 2012) largely mediates homotopic FC in Eutherian mammals. Strong causal evidence supporting the importance of the CC for mediating homotopic FC comes from cases of intractable epilepsy in which the CC was therapeutically severed (i.e., callosotomy). Pre-vs. post-operative rs-fMRI scans revealed that homotopic FC was almost completely abolished following complete callosotomy (Johnston et al., 2008) and markedly reduced following partial callosotomy (Roland et al., 2017). Long-term follow-up (2–7 years postoperative) in a subset of cases revealed no recovery of homotopic FC (Roland et al., 2017; but also see Uddin et al. (2008), a single case report of partially recovered homotopic FC 45 years postoperative, and Casimo et al. (2018), a single case report of preserved FC after incomplete anterior callosotomy). The importance of the CC as a structural mediator of homotopic FC has also been evidenced in healthy humans and macaques; specifically, the signal conduction efficacy of intact CC fibers is positively associated with homotopic FC magnitude (Shen et al., 2015; Hermesdorf et al., 2016).

Nevertheless, homotopic FC's reliance on the CC as a structural substrate appears to be somewhat region-specific, and alternative SC permits the maintenance of homotopic FC in some regions following CC damage. For example, homotopic FC between multimodal regions of frontal and parietal cortices is almost completely abolished following callosotomy, whereas homotopic FC between sensorimotor and primary visual areas is generally reduced, yet somewhat spared (O'Reilly et al., 2013; Roland et al., 2017). Parallel behavioral evidence from macaques suggests that callosotomy spares the interhemispheric transfer of simple visual information (e.g., color) but impairs interhemispheric transfer of more complex visual stimuli (e.g., visual discrimination learning tasks; Glickstein and Sperry, 1960; Glickstein et al., 1998; van der Knaap and van der Ham, 2011). It is likely that the anterior commissure (AC; Glickstein et al., 1998; Glickstein, 2009; van der Knaap and van der Ham, 2011), thalamocortical connections (Toulmin et al., 2015), and/or visuomotor transfer via the cerebellum (Glickstein et al., 1998; Glickstein, 2009; van der Knaap and van der Ham, 2011) mediates this residual interhemispheric transfer. Consistent with a potentially important role of the AC in functional adaptations following callosotomy, O'Reilly et al. (2013) noted that for a single macaque in which the CC was lesioned but the AC was spared, homotopic FC was moderately reduced, but to a lesser extent than for monkeys in which both the CC and AC were lesioned.

In examining the primacy of the CC for homotopic FC, and whether it plays a causal role, a critical distinction must be drawn between evidence obtained from callosotomy patients versus evidence obtained from individuals born without a CC (i.e., callosal dysgenesis/agenesis). Dysgenesis patients often do not exhibit the classic disconnection syndrome characteristic of callosotomy patients, a well-known purported discrepancy sometimes referred to as the Sperry paradox (Sperry, 1968; Paul et al., 2007; Tovar-Moll et al., 2014). Some dysgenesis patients exhibit reduced but not abolished homotopic FC (Quigley et al., 2003; Paul et al., 2007), and some also exhibit analogous functional deficits to callosotomy patients (Paul et al., 2007). Yet, others exhibit near normal homotopic FC and fewer behavioral deficits (Tyszka et al., 2011; Khanna et al., 2012). These mixed findings have been clarified by the discovery of aberrant long-range homotopic structural plasticity, which likely develops during a critical period for axonal targeting *in utero* (Tovar-Moll et al., 2014). In other cases, preserved homotopic FC in dysgenesis, as opposed to complete agenesis, may be attributable to partially preserved CC projections (Khanna et al., 2012; Roland et al., 2017). In sum, evidence supports a causal role for the CC in supporting homotopic FC, but also suggests that aberrant long-range structural plasticity can preserve homotopic FC in cases of CC dysgenesis, and that alternative structural pathways may be capable of at least partially compensating for loss of the CC occurring later in development.

Despite a wealth of evidence gleaned from Eutherian mammals, much less is known regarding the interhemispheric FC of either non-Eutherian mammals (e.g., opossums, platypus, etc.) or non-mammalian vertebrates (e.g., avians and amphibians), all of which lack the evolutionarily novel CC in normal ontogeny (Aboitiz and Montiel, 2003; Luo et al., 2011). Notwithstanding this, many non-mammalian vertebrates demonstrate similarly complex multimodal behaviors as Eutherian mammals, requiring a well-calibrated balance between interhemispheric coordination and hemispheric specialization, functions thought to normally be mediated by the CC (Gazzaniga, 2000; van der Knaap and van der Ham, 2011).

One such behavior is learned vocal communication. In humans, language learning is among the most complex of multimodal distributed brain processes (Geschwind, 1970), and the CC is thought to play a critical role by helping to integrate lateralized processing streams from each hemisphere (Gazzaniga, 2000). Analogously, songbirds such as the zebra finch (*Taeniopygia guttata*) exhibit vocal learning for song, a process with deep genomic, neural, behavioral, developmental, and social parallels with human speech acquisition (Doupe and Kuhl, 1999). Similar to humans, zebra finches exhibit lateralization of vocal learning and auditory processing (Cynx et al., 1992; Avey et al., 2005; Moorman et al., 2012, 2015), yet they also require tight interhemispheric coordination of premotor activity to enable vocal production (Ashmore et al., 2008). Such functional parallels between Eutherian mammals and non-mammalian vertebrates, which implicate a simultaneous need for both hemispheric specialization and interhemispheric integration, are particularly notable in light of the obvious divergence in SC (i.e., CC vs. no CC). It remains an open question whether non-mammalian vertebrates such as avians exhibit a similar pattern of homotopic FC to Eutherian mammals, despite this clear structural divergence.

Although no CC is present, the avian brain is connected bilaterally by the evolutionarily ancient AC (its largest interhemispheric connection), which connects bilateral regions of the caudal telencephalon (Letzner et al., 2016). However, in contrast to the mammalian CC, its projections are primarily heterotopically organized and unidirectional (as opposed to reciprocal), with the exception of a relatively small arcopallial and amygdaloid cluster of homotopic SC (notably, these regions are not believed to directly support song learning) (Letzner et al., 2016). Thus, the avian AC provides a less obvious structural substrate for homotopic FC compared to the CC of Eutherian mammals, or even compared to the AC of non-Eutherian mammals, which is more well-developed than the AC of some non-mammalian vertebrates, such as avians or reptiles (Heath and Jones, 1971; Aboitiz and Montiel, 2003; Letzner et al., 2016).

In addition to the AC, some polysynaptic structural pathways have been identified in songbirds which link bilateral regions of the telencephalon via interhemispheric connections within the thalamus, midbrain, and brainstem (Schmidt et al., 2006; Ashmore et al., 2008). However, these are only known to connect a small subset of premotor regions within the telencephalon (Schmidt et al., 2006; Ashmore et al., 2008). Therefore, these structural connections do not provide an obvious structural substrate for mediating the brain-wide homotopic FC commonly observed in Eutherian mammals, nor for mediating homotopic FC between a more distributed set of song network regions. It thus remains an open question whether additional polysynaptic pathways, linked to either the AC or the sub-telencephalic pathways described, might enable a more widespread distribution of homotopic FC throughout the avian brain, including additional regions of the song network.

Based on evidence obtained from callosotomy and dysgenesis patients, and the observed parallels between species for complex vocal learning, we hypothesized that the zebra finch brain would exhibit a pattern of homotopic FC similar to that of Eutherian mammals, despite lacking the CC. We performed five sets of analyses to examine this hypothesis from multiple angles. First, we tested whether homotopic FC was present within a network of well-characterized brain regions specialized for learned song. Second, we examined whether a set of subtelencephalic regions (parts of thalamus, midbrain, and hindbrain) that display direct interhemispheric SC show stronger homotopic FC than regions without homotopic SC, as is the case in Eutherian mammals (Shen et al., 2015). Third, we examined whether homotopic FC between

particular structurally connected bilateral regions was related to homotopic FC within the song network. Fourth, we complimented ROI analyses by examining homotopic FC across the whole brain using a data-driven voxel-wise analysis, a technique for which *in vivo* neuroimaging is particularly well-suited. Fifth, given that homotopic FC in humans decreases globally from childhood to middle adulthood (Zuo et al., 2010), we used a longitudinal design to investigate whether the zebra finch brain exhibits a similar developmental trajectory across the sensitive period for song acquisition. Critically, non-invasive rs-fMRI allowed us to obtain repeated measures from intact animals across development. In combination, these analyses provide the strongest test to date of the possibility that polysynaptic connections traversing interhemispheric pathways between sub-telencephalic nuclei, or relying on the largely heterotopic fibers of the avian AC, are sufficient to establish homotopic FC, absent the CC in normal ontogeny.

2. Methods

2.1. Animals

All animal procedures were approved by the Institutional Animal Care and Use Committee of the University of Chicago in accordance with the NIH Guide for the Care and Use of Laboratory Animals. Five male zebra finches (only males sing) were scanned longitudinally at four post-hatch (P) days to capture the approximate beginning, middle, and end of the song learning process (P25, P45, P65, and P90; $N = 5$ each age). A P90 MRI scan was not successfully obtained for one bird, yielding a final sample of 19 functional series. Due to scanner availability limitations, not all birds could be scanned on the exact target days: P25 (range: P24-P26), P45 (range: P44-P46), P65 (range: P64-P67), and P90 (range: P88-P91). All birds were maintained under a 14/10 h light/dark photoperiod throughout the experiment, with food provided *ad libidum*.

2.2. Scanning procedure

MRI data were collected at the MRIS Facility of the University of Chicago. Zebra finches were anesthetized using an admixture of oxygen and isoflurane gas (anesthesia induction: 1.5–2.25%; maintenance: 1–2%), administered via a tube fitted to the zebra finch beak. This procedure has been widely validated in prior zebra finch fMRI research (Boumans et al., 2007; Poirier et al., 2009, 2010; Van Ruijssevelt et al., 2013; Van Ruijssevelt et al., 2017). For example, Van Ruijssevelt et al. (2017) found that auditory-evoked BOLD responses in zebra finches are similar between isoflurane-anesthetized and awake animals. The shape of hemodynamic responses in anesthetized animals is known to be similar to that of awake animals (Shtoyerman et al., 2000; Fukuda et al., 2005; Zhao et al., 2007), and resting-state networks such as the default-mode network are well-preserved under a variety of anesthetics (Greicius et al., 2003; Vincent et al., 2007; Boveroux et al., 2010; Martuzzi et al., 2010).

Isoflurane doses varied slightly between birds within the specified range (1–2%), because we noted during pilot scans that doses <1.5% were insufficient to prevent some birds from awakening during scanning (particularly P90's), whereas doses as high as 2% posed a health hazard to some birds (particularly P25's). Thus, isoflurane doses were adjusted for each individual animal to the minimum required to maintain stable physiological readings during scanning. Notably, however, any dose adjustments nearly always occurred prior to functional acquisition, and isoflurane varied during functional acquisition for only a single bird at one time point (bird #4 at P90). We controlled for this variation in a nuisance regression described below (2.3.2. Data extraction and denoising). Isoflurane dose for each individual bird can be found in Supplementary Table S1.

Following anesthesia administration, birds were fitted with a temperature probe and respiration monitoring pad, allowing for vitals to be monitored throughout the scanning period. A previously validated feedback-controlled heating system within the scanner was used to maintain constant body temperature within the normal physiological range (~40 °C; Poirier et al., 2009, 2010; Van Ruijssevelt et al., 2013; Van Ruijssevelt et al., 2017).

2.2.1. Imaging data acquisition

Neuroimaging data were acquired using a 30 cm bore, 9.4 Tesla Bruker small animal MRI scanner. A TurboRARE-T2 multi-slice anatomical scan was acquired first during each scanning session (TR = 3.5 s, TE = 20 ms, Matrix Size: 256 × 256, in-plane resolution = 70.3 μm × 70.3 μm, slice-thickness = 200 μm, 59 slices, 9 averages). Next, resting-state spin-echo (Poirier and Van der Linden, 2011) MR images were acquired (TR = 1.07 s, TE = 27 ms (Lee et al., 1999; Jin et al., 2006; Budde et al., 2014), RARE Factor = 12 (3 repetitions per acquisition), Matrix Size: 128 × 36, in-plane resolution = 141 μm × 500 μm, slice-thickness = 750 μm, 15 slices). Slices were acquired in an interleaved, ascending order. 180 vol were acquired consecutively with an effective sampling rate of one volume per 3.20 s and a total resting-state scan time of 9.60 min. To avoid T1-equilibration effects, the first five volumes of each functional series were discarded.

The sampling rate utilized represented a trade-off between image structural resolution, full brain coverage, and scanner limitations, versus temporal resolution. Although our sampling rate was slower than the two-second TR often used in human neuroimaging studies, it still easily met the Nyquist criterion for alias free signal sampling. Specifically, for a bandwidth of 0.092 Hz (0.008–0.10 Hz passband), which is commonly used to define resting-state fMRI frequencies of interest, a Nyquist rate of 0.184 Hz (2 times the bandwidth, equivalent to one sample every 5.43 s) is needed to successfully resolve the underlying function without aliasing. It is also worth noting that the fastest of the slow hemodynamic fluctuations measured in the resting-state (0.1 Hz) complete one cycle every 10 s.

2.2.2. Preprocessing

Image preprocessing was completed using a combination of Advanced Normalization Tools (ANTs; Avants et al., 2009, 2011), Statistical Parametric Mapping (SPM12; Penny et al., 2011), and custom Matlab scripts. First, DICOM files were converted to NIfTI format using our MRIqual toolbox (E.A.L., in preparation). Second, the "N4" bias field correction algorithm (Tustison et al., 2010) was used to correct images for magnetic field intensity inhomogeneity. Third, an average of the bias-corrected anatomical scans was selected as an unbiased starting point for symmetric group-wise normalization (SyGN; Avants et al., 2010) and template-building using ANTs. This process involved iteratively registering each anatomical scan to a custom brain template using affine and nonlinear transformations. As image registration improved, the custom template was recursively updated in each iteration. Cross-correlation was implemented as the similarity metric for image comparison, and four template construction iterations were completed.

Fourth, functional scans were corrected for slice timing differences using SPM (Johnstone et al., 2006; Sladky et al., 2011). Fifth, each 3D functional volume was realigned to the first volume in its series using ANTs, and the six rigid-body motion parameters were retained for later nuisance regression. Sixth, the first functional volume of each series was co-registered to the corresponding bias-corrected anatomical volume via affine transformation in ANTs. To minimize the number of interpolations applied, all affine and nonlinear transformations obtained from functional realignment, coregistration, and structural normalization were combined into 3D volume-specific deformation fields using the ANTs routine "antsApplyTransforms." Seventh, deformation fields were applied in a single step to each slice timing corrected 3D functional volume. Lastly, we assessed the quality and consistency of spatial normalization by computing voxel-wise Pearson correlations between the custom template and normalized anatomical scans across voxels ($r_{mean} = 0.94$, $SD = 0.01$, $r_{min} = 0.91$), as well as between the normalized functional scans averaged across time and the custom template

($r_{mean} = 0.87$, $SD = 0.02$, $r_{min} = 0.81$). These analyses indicated a robust and consistent spatial normalization across scans.

2.3. Data preparation

2.3.1. Region of interest (ROI) delineation

Using our open-source NeuroViz toolbox for Matlab (E.A.L. & M.G.B., in preparation), coauthor S. E. L. manually delineated six key components of the zebra finch song network within each hemisphere on our anatomical brain template using anatomical references and a previously published zebra finch brain atlas (Poirier et al., 2008). These regions of interest (ROIs) included two sensory processing areas (1. Field L and 2. auditory forebrain (here defined as caudomedial nidopallium (NCM) and caudal mesopallium (CM)), three sensorimotor regions (1. lateral magnocellular nucleus of the anterior nidopallium (LMAN), 2. Area X, and 3. HVC (used as a proper name)), and one premotor region (1. robust nucleus of the arcopallium (RA)). Tract tracing studies have indicated that these regions do not exhibit homotopic SC (Wild et al., 1997; Striedter and Vu, 1998; Schmidt et al., 2006; Ashmore et al., 2008), and therefore they will henceforth be referred to as "homotopic non-structurally connected" (*homotopic-nSC*) ROIs. We also delineated four additional bilateral ROIs that include brain areas known to receive bilateral inputs and/or direct homotopic SC: the medulla, medial diencephalon, thalamic nucleus uvaeformis (Uva), and the dorsomedial subdivision of the intercollicular nucleus (DM) (Ashmore et al., 2008; Striedter and Vu, 1998; Wild et al., 1997; Wild et al., 2000). These latter ROIs will henceforth be referred to as "homotopic structurally connected" (*homotopic-SC*) ROIs. For further details on the homotopic SC of

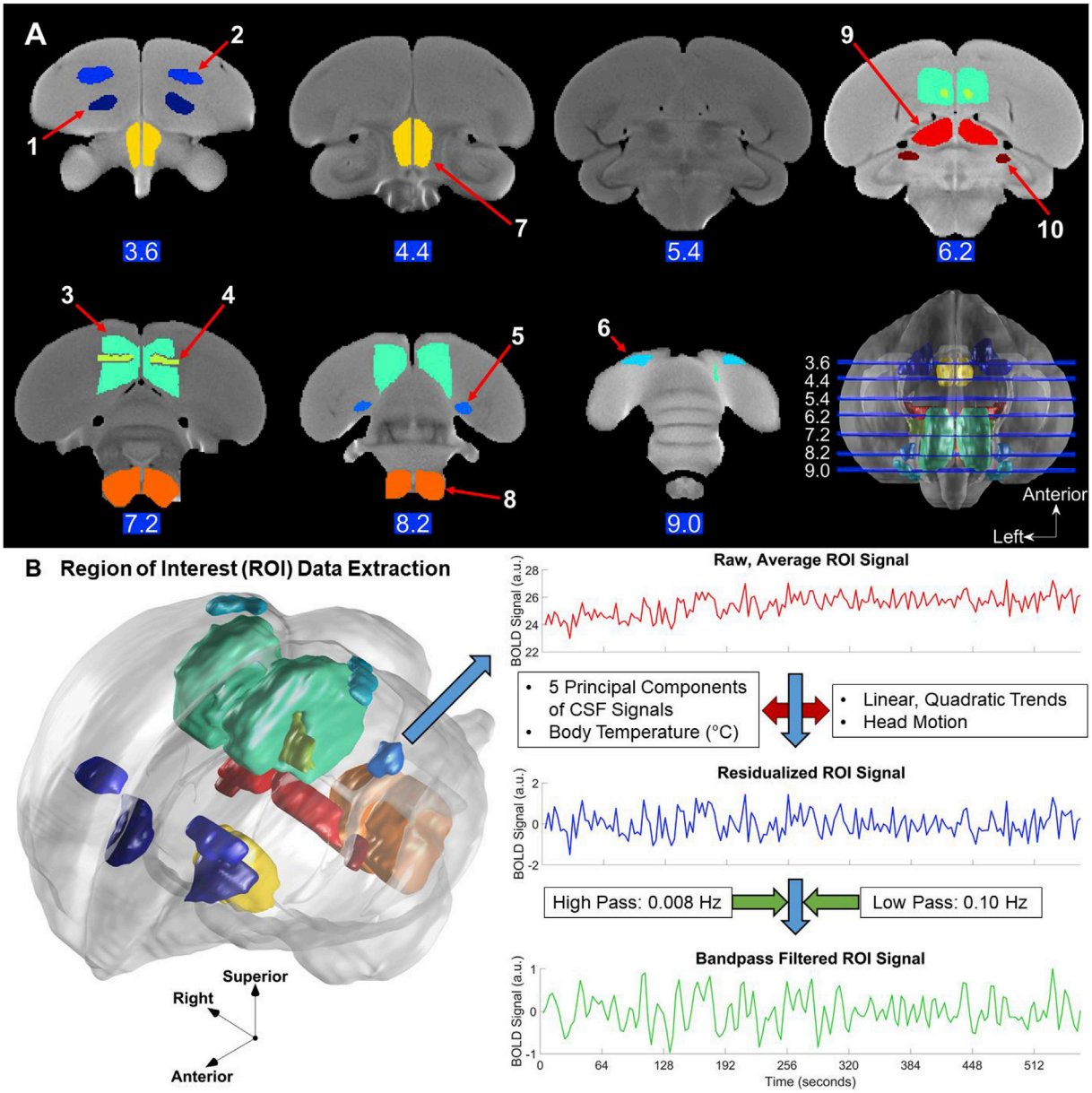

Fig. 1. Region of interest (ROI) delineation and preprocessing. **A:** Slice mosaic of the male zebra finch brain template overlaid with ROIs (**Song Network:** 1. Area X (*Midnight Blue*); 2. LMAN (*Royal Blue*); 3. Auditory Forebrain (*Light Green*); 4. Field L (*Light Yellow*); 5. RA (*Blue*); 6. HVC (*Teal*); **Homotopic-SC ROIs: 7.** Medial Diencephalon (*Yellow*); 8. Medulla (*Orange*); 9. Uva (*Red*); 10. DM (*Maroon*)). The brain slices shown are 3.6, 4.4, 5.4, 6.2, 7.2, 8.2, and 9.0 mm from the anterior tip of the telencephalon. **B:** *Left:* ROIs displayed within a 3D rendering of the male zebra finch brain template. 3D axes show brain orientation. *Right:* The basic data extraction and preprocessing steps are shown using data from left RA in male 1 at P25. Signals extracted from all voxels of an ROI were averaged (top), nuisance regression was performed (middle), and ROI signals were bandpass filtered (bottom).

these regions, see Supplementary Materials. This procedure yielded twenty ROIs in total, comprised of ten bilateral homotopic pairs (Fig. 1A, Supplementary Table S2). Finally, in addition to these ROIs, co-author S. E. L. manually traced a conservative cerebrospinal fluid (CSF) mask, comprised of voxels within brain ventricles.

2.3.2. Data extraction and denoising

Data extraction and denoising were accomplished using custom Matlab scripts and NIfTI Tools (Shen, 2014) for loading and saving NIfTI files. For each resting-state functional series, BOLD time series were extracted from the voxels comprising each ROI and averaged. We followed the default approach used in CONN Toolbox (Whitfield-Gabrieli and Nieto-Castanon, 2012) by extracting ROI signals from unsmoothed functional data, so as to avoid contamination of the ROI signals with signal from neighboring regions. However, our main results were robust to using either unsmoothed or smoothed functional data for ROI extraction (Supplementary Materials, section 6). Next, a nuisance regression was performed in which the six rigid body motion parameters (Bright and Murphy, 2015), the first five principal components of CSF signals (Behzadi et al., 2007; Whitfield-Gabrieli and Nieto-Castanon, 2012; Layden et al., 2017), linear and quadratic trends (Tanabe et al., 2002), and body temperature were removed from each ROI time series. The residual ROI time series were then bandpass filtered (range: 0.008–0.1 Hz; Hallquist et al., 2013) using the bst_bandpass_filtfilt function from Brainstorm (Tadel et al., 2011). See Fig. 1B for a visual depiction of this process.

2.4. rs-fMRI validation analyses

2.4.1. Temporal signal-to-noise ratio (tSNR)

The quantification of image quality metrics such as the temporal signal-to-noise ratio (*tSNR*) may be particularly valuable for novel scanning paradigms and/or for use with model organisms, for which scanning parameters are often less well-established (Kalthoff et al., 2011). We calculated *tSNR* voxel-wise, using MRIqual, as the temporal mean intensity divided by the temporal standard deviation (Triantafyllou et al., 2005; Harmer et al., 2012; Kemper et al., 2015). *tSNR* values were averaged across all voxels within the brain mask to summarize whole-brain *tSNR*.

Spatial smoothing is known to markedly enhance *tSNR* (Molloy et al., 2014), and many studies only report *tSNR* for either smoothed or unsmoothed data (e.g., Harmer et al., 2012; Chang et al., 2018). This factor (and heterogeneous smoothing protocols) may help to account for the wide variability observed in *tSNR* values in prior literature (range: [4.42, 280], Welvaert and Rosseel, 2013). Therefore, to enable easier comparison to prior studies, we calculated whole-brain *tSNR* for both unsmoothed and smoothed ($0.422 \times 1.000 \times 1.125$ mm FWHM, corresponding to 3 × 2 x 1.5 voxels, respectively) rs-fMRI scans. We then compared *tSNR* values from this study to those obtained in prior studies utilizing sub-millimeter voxel resolutions at high magnetic field strengths (Barth and Norris, 2007; Desai et al., 2010; Kemper et al., 2015; Liska et al., 2015; Yoshida et al., 2016; Rua et al., 2017; Chang et al., 2018; Huber et al., 2018). Given the small volume of our functional voxels (~0.05 mm^3), *tSNR* was expected to be lower than in human resting-state scans collected at lower spatial resolution (i.e., more coarse), because *tSNR* is known to be strongly related to voxel volume (i.e., larger voxel volume yields higher *tSNR*; Triantafyllou et al., 2005; Murphy et al., 2007; Hutton et al., 2011; Zwaag et al., 2012).

2.4.2. Power spectral analyses

The power spectrum for each resting-state functional series was calculated within the infra-slow frequency range (~0.008–0.1 Hz; Cordes et al., 2001) after the completion of preprocessing. Average power was calculated via Welch's power spectral density estimate, implemented using the Matlab function pwelch.m and integrated within MRIqual. The power spectrums obtained were compared to those reported in the human resting state literature (Duff et al., 2008; Kim et al., 2014) and in the murine literature, which routinely utilizes isoflurane anesthesia (Kannurpatti et al., 2008; Grandjean et al., 2014). Both literatures have consistently identified $1/f$ power spectrums, with resting-state power highest in low frequency bands (<0.1 Hz). In particular, resting-state time series obtained from isoflurane anesthetized mice (Grandjean et al., 2014) and rats (Kannurpatti et al., 2008) have demonstrated peaks in the power spectrum at very low frequencies (~0.01 Hz).

2.4.3. FC of anatomical connections

Anatomical connectivity is known to moderately predict FC at rest in humans (Honey et al., 2009). However, distinct brain networks are associated with the resting-state as compared to various task states (Greicius et al., 2003). Therefore, it is uncertain to what extent we might expect to observe FC between previously delineated premotor and motor pathways during the resting-state. However, we proceeded to investigate whether there was consistency between the FC measured in the present study and SC known from prior research.

In particular, an ipsilateral projection from HVC to RA comprises an important component of the descending motor pathway for song production, and this anatomical connection has been observed previously using diffusion tensor imaging (DTI) in starlings (De Groof et al., 2006). Notably, projections from HVC to RA do not project into RA until after ~ P30, and they are thought to increase in density and conduction efficacy from P30 to adulthood (≥P90; Mooney and Rao, 1994). Therefore, we restricted our search for any analogous FC between HVC and RA to birds P45 or older, and we additionally investigated whether FC increased with age.

Another widely studied anatomical pathway is the projection from LMAN to RA, a connection crucial for song learning during development but less involved in stereotyped song production during adulthood (Aronov et al., 2008). This projection is known to be present as early as P15 (Mooney and Rao, 1994) but becomes functionally less important as song becomes crystalized (Aronov et al., 2008). We thus investigated whether FC between LMAN and RA was present across all ages. Finally, we also investigated FC between another prominent ipsilateral structural connection between Field L (primary auditory region) and auditory forebrain (secondary auditory region) (Vates et al., 1996).

We utilized one-sample *t*-tests to determine whether FC was positive and significant across birds for these known structural connections. Also, we used a linear mixed-effects (LME) model to examine the fixed-effect of age on HVC to RA FC, controlling for a random intercept for bird. Additional investigations of known ipsilateral projections are detailed in Supplementary Materials (Section 1, Table S4).

2.5. Homotopic FC analyses

ROI-to-ROI FC was computed separately for each bird at each age. FC was defined as the Fisher's *Z*-transformed Pearson correlation between the preprocessed time series of a pair of ROIs. This FC measure reliably detects homotopic FC in Eutherian mammals (Stark et al., 2008; Zuo et al., 2010; Shen et al., 2015) and provides results consistent with alternative measures of brain connectivity (Pan et al., 2011; Matsui et al., 2016).

We first sought to determine whether homotopic FC is relatively stronger than ipsilateral or heterotopic FC across the ROIs of the zebra finch brain, as has been shown consistently in Eutherian mammals. To do so, we implemented an LME random-intercept model in which ROI-to-ROI FC across all ROIs served as the criterion variable. Connection type (homotopic, heterotopic, and ipsilateral) was entered as a three-level nominal fixed-effect, with ipsilateral coded as the reference category. We also controlled for the fixed-effect of age and included a random intercept for bird to account for repeated measures. This LME model was optimized for maximum likelihood using the Matlab function "fitlme." A contrast was performed for the effect of homotopic vs. ipsilateral FC. We then redefined heterotopic as the reference category for the connection

type variable, so that an effect size for the homotopic vs. heterotopic FC contrast could also be estimated. Finally, we also report the main effect of connection type based on a likelihood-ratio drop-test.

2.5.1. Additional controls

We sought to control for a variety of nuisance factors known to influence resting-state FC. For instance, the Euclidean distance between a pair of ROIs is known to be inversely associated with the FC strength of the pair (Salvador et al., 2005; Honey et al., 2009; Mišić et al., 2014). Additionally, increased ROI volume is associated with increased FC strength (Salvador et al., 2008; Wang et al., 2009). Therefore, we added these covariates to our previously described LME model. Additionally, we added isoflurane dose and average body temperature over the duration of functional acquisition as additional covariates for our LME model.

2.5.2. FC of individual homotopic connections

To examine whether homotopic FC was specific to a subset of ROIs or presented as a more global feature of the zebra finch brain, we computed one-sample *t*-tests to determine whether the FC of each individual homotopic ROI pair significantly differed from zero across birds and ages. We corrected for multiple comparisons across homotopic connections using the false discovery rate (FDR). Next, we constructed a grand mean ROI-to-ROI FC network by averaging Fisher's *Z* values across birds and ages (Fig. 2). This grand mean FC network was thresholded at $p < 0.05$ for display purposes.

2.5.3. Isoflurane and homotopic FC

Our analyses above examined whether homotopic FC was stronger than ipsilateral or heterotopic FC, controlling for any effect of isoflurane dose. Interestingly, however, a recent study found that increasing isoflurane dose from 1.1 to 2% selectively and causally decreased homotopic FC in mice (Bukhari et al., 2018), consistent with prior correlational results in rats (Hutchison et al., 2014). Thus, we added the interaction between connection type and isoflurane dose to our LME model to determine whether increasing isoflurane dose was associated with selectively reduced homotopic FC in the zebra finch.

2.6. Homotopic-SC vs. homotopic-nSC

In humans and macaques, homotopic FC appears to depend on the direct SC of the CC (Quigley et al., 2003; Johnston et al., 2008; Shen et al., 2015; Roland et al., 2017). Thus, to gauge whether homotopic SC also serves to augment homotopic FC in the zebra finch brain, we examined whether FC was significantly stronger between homotopic-SC ROI pairs compared to homotopic-nSC ROI pairs. We implemented an LME model, here considering only the FC of homotopic connections. Connection type was added as a binary categorical variable (homotopic-SC vs. homotopic-nSC), and age and a random intercept for bird were included as covariates. In a follow-up regression, we also included the covariates described in "Additional controls."

2.6.1. Test for mediation of homotopic-nSC FC by homotopic-SC FC

A minority of ipsilateral anatomical connections have been identified that connect homotopic-SC and homotopic-nSC ROIs (Schmidt et al., 2006; Ashmore et al., 2008). Therefore, a natural question is whether FC between homotopic-SC ROIs might indirectly mediate the homotopic FC observed between homotopic-nSC ROI pairs. In particular, the thalamic nucleus Uva is known to make direct ipsilateral projections to HVC while receiving direct bilateral inputs from DM (a midbrain nuclei) and PAm (a medullary nuclei; Schmidt et al., 2006; Ashmore et al., 2008). This circuit is thought to be critical for enabling the interhemispheric coordination of descending motor output for song production (Schmidt et al., 2006; Ashmore et al., 2008; Hamaguchi et al., 2016; Galvis et al., 2018), although little is known regarding its role in the interhemispheric coordination of intrinsic brain activity. Therefore, we sought to investigate whether Uva homotopic FC or Uva-HVC FC might mediate HVC homotopic FC, as this connection in particular appeared to be the most likely candidate for the mediation of homotopic-nSC FC by homotopic-SC FC. To investigate this possibility, we first undertook a series of bivariate correlation analyses, examining whether the homotopic FC of bilateral HVC was correlated with 1. R Uva to R HVC ipsilateral FC, 2. L Uva to L HVC ipsilateral FC, 3. Uva homotopic FC, 4. the interaction between Uva homotopy and R Uva to R HVC FC, or 5. the interaction between Uva homotopy and L Uva to L HVC. If merited by the results of this analysis, we planned to subsequently undertake more extensive regression-based mediation analyses.

2.7. Homotopy as a function of development

In human subjects, global homotopic FC decreases from early childhood through middle adulthood, a trend which may reflect the development of increasing hemispheric specialization (Zuo et al., 2010). Thus, we investigated whether a similar trajectory of changes in homotopic FC might be observed in zebra finches across the developmental time-course of song learning. To do so, we added a term denoting the interaction between age and connection type (Homotopic, Ipsilateral, and Heterotopic) to the LME model described above in section 2.5. We then conducted a follow-up analysis in which we parsed the homotopic connection type into Homotopic-SC and Homotopic-nSC to investigate whether age effects were specific to either type.

2.8. Full model predicting ROI-to-ROI FC

Finally, to examine homotopic FC when comprehensively controlling for all effects and interactions investigated in previous sections, we implemented an LME model which included all of the following fixed-effects covariates: (1) connection type (homotopic-nSC, homotopic-SC, ipsilateral, heterotopic), (2) age, (3) body temperature, (4) isoflurane dose, (5) Euclidean distance, (6) ROI volume, (7) connection type by age interaction, and (8) connection type by isoflurane dose interaction. Additionally, a random intercept was included for bird. We examined whether this model could be further reduced to minimize AIC.

2.9. Voxel-wise homotopic FC

To further interrogate the distribution of homotopic FC agnostically, without pre-defined ROIs, we implemented the experimenter-blind voxel-mirrored homotopic connectivity (VMHC; Zuo et al., 2010) analysis, using a combination of custom Matlab scripts, SPM12, the Data Processing & Analysis for (Resting-State) Brain Imaging (DPABI) toolbox, and ANTs. VMHC analysis allowed us to characterize the voxel-wise distribution of homotopic FC across the entire brain. Specifically, VMHC quantifies FC between each voxel in one hemisphere with its mirror-symmetric counterpart in the contralateral hemisphere. The VMHC analysis proceeded as follows: first, a symmetric group-wise brain template was formed by mirroring the right hemisphere of our custom brain template across the midline. Each individual anatomical scan was then renormalized to this symmetric brain template. The transformation parameters obtained from normalization were then applied to each corresponding functional series, using ANTs. Subsequently, each functional scan was smoothed using a Gaussian kernel ($0.422 \times 1.000 \times 1.125$ mm FWHM, corresponding to 3×2 x 1.5 voxels in functional dimensions) in SPM12 to help account for any registration errors and/or individual-specific brain anatomy. Spatial smoothing may be especially critical for VMHC analysis, given that VMHC compares pairs of symmetric voxels, requiring great spatial precision (Zuo et al., 2010). Additionally, sufficient spatial smoothing is an important assumption of random-field theory-based methods (Eklund et al., 2016) and helps to overcome potential errors in registration and realignment (Mikl et al., 2008).

Next, Fisher's *Z*-transformed Pearson correlations were computed between each pair of homotopic brain voxels, and voxel-wise *t*-statistics were calculated to summarize the strength of homotopic FC across birds and time points. Finally, all voxels within a distance of 0.281 mm (i.e.,

four structural voxels, two functional voxels) from either side of the midline were set to zero to avoid obtaining artefactual homotopic FC as a result of spatial smoothing (for FWHM = 0.422 mm, $\sigma \cong 0.179$ mm, yielding an approximate cut-off for signal contamination at $3\sigma = 0.537$ mm, corresponding to 7.64 structural voxels or 3.82 functional voxels).

Significant clusters of homotopic FC were detected using the cluster-extent based thresholding method, as implemented in the DPABI toolbox (primary/voxel-level threshold: *p-uncorrected* < 0.001, family-wise error (FWE)-corrected cluster-extent threshold: *pFWE* < 0.05; Yan et al., 2016). By illuminating regional clusters of homotopic FC, such an analysis has the potential to be informative for future studies investigating putative neural pathways underlying interhemispheric coordination in the avian brain. We next calculated the overlap between significant homotopic FC clusters and our previously delineated homotopic-nSC song ROIs as the number of intersecting voxels divided by the total number voxels included within homotopic-nSC ROIs. To compare this overlap to chance, we utilized a permutation test in which the voxel indices of homotopic FC clusters were randomly permuted 10,000 times, and the proportion of overlap with our homotopic-nSC ROIs was calculated in each case. The original observed overlap proportion was then compared to the null distribution of overlap proportion obtained via permutations to derive a non-parametric *p*-value.

2.9.1. Quantitative comparison of voxel-wise homotopic vs. ipsilateral and heterotopic FC

In addition to examining the regional distribution of homotopic FC, we also sought to quantitatively compare the distribution of voxel-wise homotopic FC to the distributions of voxel-wise ipsilateral and heterotopic FC, in a manner similar to what was done previously for ROI-based analyses. Therefore, we calculated the average voxel-wise FC for each connection type (homotopic, ipsilateral, heterotopic) for each bird, and at each time point. This allowed us to fit a mixed-effects random intercept model in which average FC served as the criterion variable, and fixed-effects predictors were connection type, age, isoflurane dose, and body temperature; a random intercept was included for bird. We examined the main effect of connection type using a likelihood-ratio drop-test, and then we examined the simple effect contrasts for homotopic vs. other connection types. For reference, we also computed the effect size (as Cohen's *d*) of the difference between all voxel-wise homotopic connections and ipsilateral or heterotopic connections across birds. In supplementary materials, we provide this same effect size measure for each individual scan (Supplementary Table S7).

2.9.2. Full model for voxel-wise FC

Finally, we replicated the optimal model for predicting ROI FC (section 3.5, Table 1) using average voxel-wise FC. Euclidean distance and ROI volume were ROI-specific measures, and they could not be used in this case given that the criterion variable here was average voxel-wise FC across the whole brain. We therefore implemented an LME random intercept model which included all of the following fixed-effects: (1) connection type (homotopic, ipsilateral, reference: heterotopic), (2) age, (3) body temperature, (4) isoflurane dose, (5) a connection type by age interaction, and (6) a connection type by isoflurane dose interaction. Additionally, a random intercept was included for bird. We examined whether this model could be further reduced to minimize AIC.

2.10. Figure creation

Figs. 1–5 were created using our NeuroViz Toolbox (E.A.L. & M.G.B., in preparation) and custom Matlab scripts.

2.11. Data and code availability statement

Key fMRI data, analysis code, ROI masks, and the custom group-wise brain template are all openly available from our G-Node Open Data repository (https://doi.org/10.12751/g-node.6b6170).

3. Results

3.1. rs-fMRI validation analyses

3.1.1. tSNR

Across functional scans, *tSNR* (smoothed: $M = 58.37$, $SD = 13.22$; unsmoothed: $M = 15.22$, $SD = 2.81$; Supplementary Table S3) was comparable to values reported in prior research utilizing sub-millimeter voxel resolutions at high magnetic field strengths. For example, three mouse studies reported similar *tSNR* values for smoothed data (e.g., $tSNR = 27.7 \pm 5.8$, Chang et al., 2018; $tSNR = 23$–40, Liska et al., 2015; $tSNR = 53 \pm 4$, Yoshida et al., 2016). Also, one mouse study ($tSNR = 15$–17, Desai et al., 2010) and four human studies ($tSNR = 15$–20, Barth and Norris, 2007; $tSNR = 18 \pm 4$, Huber et al., 2018; $tSNR \approx 5$–15, Kemper et al., 2015; $tSNR \approx 10$, Rua et al., 2017) reported similar *tSNR* values for unsmoothed data.

3.1.2. Power spectral analyses

Consistent with prior rs-fMRI data, the zebra finch rs-fMRI signals exhibited power spectrums with a $1/f$ (frequency) distribution, with the highest power at low frequencies (Supplementary Fig. S1; Kannurpatti et al., 2008; Grandjean et al., 2014). Specifically, this observation concerns the relative distribution of power within the resting-state frequency range and not necessarily between the resting-state and non-resting-state frequency ranges.

3.1.3. FC of anatomical connections

We next examined FC between brain regions known to be connected by ipsilateral SC from invasive tract tracing studies (Supplementary Materials, Section 1; Table S4). We noted a trend toward positive FC for L HVC – L RA, an important component of the descending motor pathway for song production, for birds aged P45-90 ($t(13) = 1.82$, $p = 0.092$). Interestingly, the FC of this connection increased significantly with age, from P25 through P90 ($B = 0.47$, $t(17) = 2.33$, $p = 0.032$), consistent with its previously characterized structural developmental trajectory (Mooney and Rao, 1994). However, FC was not significant for the right hemispheric homologue of this connection ($t(13) = 0.23$, $p > 0.80$), nor was there a significant trend with age ($B = 0.03$, $t(17) = 0.13$, $p > 0.80$). We also found that Field L and Auditory Forebrain exhibited robust ipsilateral FC in both hemispheres across birds (R Field L – R Aud. Forebrain: $t(18) = 12.30$, $p < 0.001$; L Field L – L Aud. Forebrain: $t(18) = 6.85$, $p < 0.001$). Notably, despite their close spatial proximity, these ipsilateral connections remained significant after regressing out the effects of Euclidean distance across connections (R Field L – R Aud. Forebrain: $t(18) = 12.80$, $p < 0.001$; L Field L – L Aud. Forebrain: $t(18) = 7.17$, $p < 0.001$). Finally, we failed to find significant FC for LMAN to RA in either hemisphere (both $p > 0.45$). Additional analyses investigating the FC of known structural connections are detailed in Supplementary Materials (Supplementary Table S4).

3.2. Homotopic functional connections are among the strongest within the song network

To test our first hypothesis, that homotopic FC would be observed among a set of distributed regions important for learned song, we analyzed homotopic FC across the homotopic-nSC regions of the song network. We fit an LME random intercept model predicting ROI-to-ROI FC via connection type (homotopic, ipsilateral, heterotopic), controlling for age and bird-specific effects. This revealed a strong main effect of connection type as evidenced by a likelihood-ratio drop-test ($\chi^2(2) = 91.33$, $p < 0.001$), such that homotopic connections were significantly stronger than either ipsilateral ($B = 0.15$, $t(1250) = 9.08$, $p < 0.001$) or heterotopic connections ($B = 0.16$, $t(1250) = 9.50$, $p < 0.001$). This effect was not explained by the Euclidean distance

between ROIs, the average volume of ROI pairs, isoflurane dose, or body temperature. The FC strength of homotopic connections remained higher than that of the other connection types after controlling for these nuisance variables (homotopic vs. ipsilateral: $B = 0.17$, $t(1246) = 10.62$, $p < 0.001$; homotopic vs. heterotopic: $B = 0.12$, $t(1246) = 7.45$, $p < 0.001$), and the main effect of connection type remained significant ($\chi^2(2) = 109.45$, $p < 0.001$).

We next analyzed the FC of individual homotopic ROI pairs. One-sample *t*-tests revealed significant positive FC among all homotopic ROI pairs after correction for multiple comparisons using FDR. Average homotopic FC values (mean Fisher *Z*-transformed correlations) and FDR-corrected *p*-values (*pFDR*) were as follows: Area X ($Z = 0.19$, $pFDR < 0.001$), LMAN ($Z = 0.17$, $pFDR = 0.001$), RA ($Z = 0.06$, $pFDR = 0.012$), HVC ($Z = 0.16$, $pFDR = 0.002$), Auditory Forebrain ($Z = 0.48$, $pFDR < 0.001$), and Field L ($Z = 0.15$, $pFDR = 0.001$). Fig. 2 displays FC values for the entire song network thresholded at $p < 0.05$ for display purposes.

3.2.1. Isoflurane and homotopic FC

Although the main effect of isoflurane dose was not significant in the model described above in section 3.2 ($B = -0.02$, $t(1246) = -1.29$, $p > 0.19$), we next examined whether isoflurane dose interacted with connection type, as has been found in prior literature. We found that the overall interaction between isoflurane dose and connection type, as measured by a likelihood-ratio drop-test, was significant ($\chi^2(2) = 8.24$, $p = 0.016$). Higher isoflurane doses were associated with selectively lower homotopic FC, relative to either ipsilateral ($B = -0.12$, $t(1244) = -2.41$, $p = 0.016$) or heterotopic FC ($B = -0.14$, $t(1244) = -2.87$, $p = 0.004$). In contrast, isoflurane dose was not differentially associated with heterotopic versus ipsilateral FC ($B = -0.02$, $t(1244) = -0.80$, $p > 0.40$). Notably, Homotopic FC remained stronger than ipsilateral ($B = 0.42$, $t(1244) = 4.64$, $p < 0.001$) or heterotopic ($B = 0.34$, $t(1244) = 3.69$, $p < 0.001$) FC after controlling for the interaction between isoflurane dose and connection type.

3.3. Structural connectivity predicts greater homotopic FC in zebra finches

As expected, all homotopic-SC ROIs exhibited significant homotopic FC (all $pFDR < 0.05$; Fig. 2). More interestingly, homotopic-SC connections demonstrated significantly stronger FC than homotopic-nSC connections ($B = 0.10$, $t(187) = 2.97$, $p = 0.003$; Fig. 3) even after controlling for nuisance covariates ($B = 0.07$, $t(183) = 2.18$, $p = 0.030$).

3.3.1. No evidence that homotopic-SC connections mediate homotopic-nSC connections

Across zebra finches, HVC homotopic FC was uncorrelated with: 1. R Uva to R HVC ipsilateral FC ($r(17) = -0.01$, $p > 0.90$), 2. L Uva to L HVC ipsilateral FC ($r(17) = -0.16$, $p > 0.50$), 3. Uva homotopic FC ($r(17) = 0.18$, $p > 0.45$), 4. the interaction between Uva homotopy and R Uva to R HVC FC ($r(17) = 0.12$, $p > 0.60$), and 5. the interaction between Uva homotopy and L Uva to L HVC FC ($r(17) = -0.09$, $p > 0.70$). Thus, our results offered no indication that the FC of homotopic-SC ROIs, specifically involving Uva, mediated the homotopic FC of HVC. As such, we did not consider these results to merit more extensive regression-based mediation analyses.

3.4. Homotopy as a function of development

To investigate the developmental trajectory of homotopic FC, we added an age by connection type interaction to the random intercept model described in section 3.2, again controlling for effects of Euclidean distance between ROIs, the average volume of ROI pairs, isoflurane dose, and body temperature. The interaction main effect was significant, as evidenced by a likelihood-ratio drop-test ($\chi^2(2) = 6.95$, $p = 0.031$). Consistent with human findings, zebra finch homotopic FC decreased significantly more with age than did ipsilateral ($B = -0.0012$, $t(3600) = -2.59$, $p = 0.010$) or heterotopic ($B = -0.0010$, $t(3600) = -2.10$, $p = 0.035$) FC. In contrast, heterotopic and ipsilateral FC did not developmentally differ ($B = -0.0002$, $t(3600) = -1.08$, $p > 0.25$).

A follow-up analysis, in which homotopic connections were parsed into homotopic-SC and homotopic-nSC sub-types, again revealed a significant age by connection type interaction ($\chi^2(3) = 16.09$, $p = 0.001$). Interestingly, analysis of simple effects revealed that homotopic-SC connections decreased significantly with age ($B = -0.0028$, $t(3598) = -3.98$, $p < 0.001$), whereas homotopic-nSC connections did not ($B = -0.0001$, $t(3598) = -0.20$, $p > 0.80$).

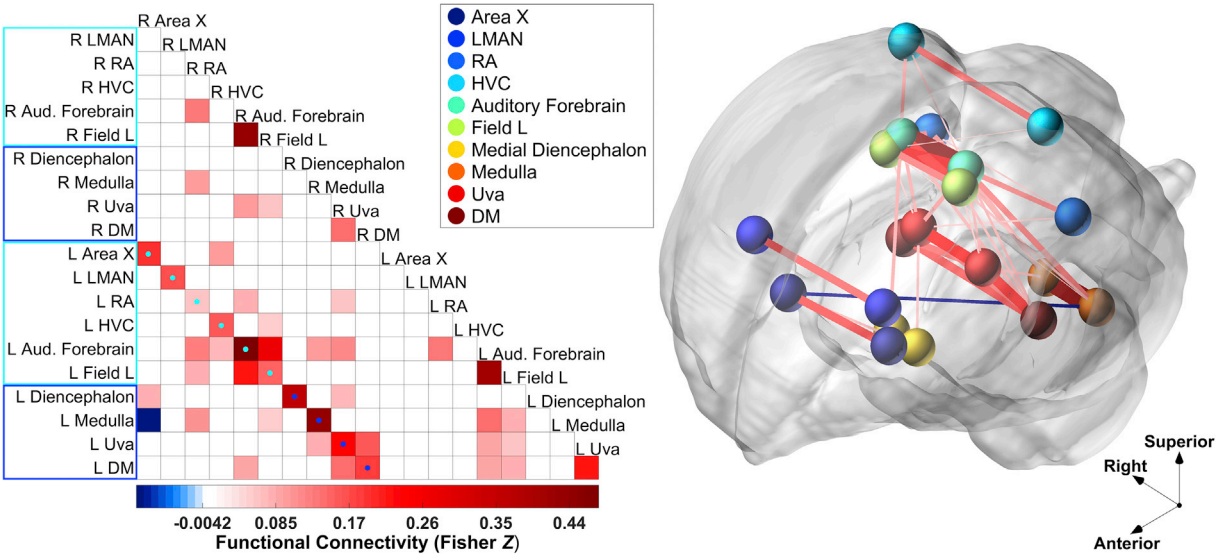

Fig. 2. A prominent pattern of homotopic FC. *Left:* The grand mean FC matrix thresholded at *p-uncorrected* < 0.05. The blue-red color scale corresponds to average Fisher *Z*-transformed Pearson product-moment correlations across birds and ages. Homotopic connections are displayed on the diagonal highlighted by teal and blue dots. Teal boxes and dots: the song network ROIs (no direct homotopic SC) and homotopic connections, respectively. Blue boxes and dots: homotopic-SC ROIs and homotopic connections, respectively. *Right:* The grand mean FC network overlaid on a 3D rendering of the group-average brain template. Spheres are located at the centroids of each corresponding ROI listed in the legend. Connections depict the Fisher *Z* values (left panel), with both line thickness and color proportional to the association strength. 3D axes show brain orientation.

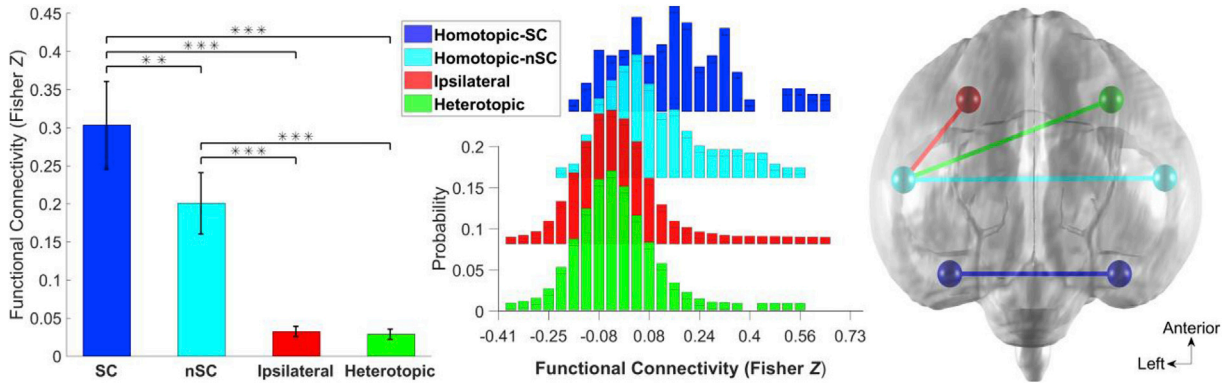

Fig. 3. The relative FC of different connection types. *Left:* Bar plot showing mean FC values as Fisher Z-transformed Pearson product-moment correlations apportioned by connection type. Error-bars represent 95% confidence intervals. *** = $p < 0.001$, ** = $p < 0.01$. Effect sizes for the contrast between homotopic-SC and other connection types were as follows: $d = 0.44$ (homotopic-nSC), $d = 1.77$ (ipsilateral), $d = 1.89$ (heterotopic). Effect sizes for the contrast between homotopic-nSC and other connection types were as follows: $d = 1.10$ (ipsilateral), $d = 1.19$ (heterotopic). *Middle:* Histograms showing the distribution of FC values for each connection type. Histogram bins were normalized as the probability of FC of a given magnitude for each connection type. *Right:* A schematic illustrating each connection type overlaid on a superior view of the zebra finch brain template. Axes show brain orientation.

3.5. Full model

Finally, to examine homotopic FC when comprehensively controlling for all fixed-effects and interactions investigated in previous sections, we implemented an LME model which included all of the following fixed-effects covariates: (1) connection type (homotopic-nSC, homotopic-SC, ipsilateral, heterotopic), (2) age, (3) body temperature, (4) isoflurane dose, (5) Euclidean distance, (6) ROI volume, (7) connection type by age interaction, and (8) connection type by isoflurane dose interaction. Additionally, a random intercept was included for bird. We found that this model was not further reducible based on AIC (i.e., AIC was increased by removing any predictor). Model parameters are displayed in Table 1 below.

3.6. A medially-biased, brain-wide pattern of homotopic FC

VMHC analyses revealed a distributed pattern of homotopic FC, notably similar to the voxel-wise pattern observed in the human brain (Stark et al., 2008; Zuo et al., 2010). For example, homotopic FC appeared to be more pronounced within medial portions of the zebra finch brain (Zuo et al., 2010), spanning the medulla to the superior telencephalon, with lesser homotopic FC observable in more lateral regions (Fig. 4). Similar to the findings of Zuo et al. (2010) in humans, a single, large significant cluster of homotopic FC was identified which encompassed 87.8% of the total brain volume (primary threshold: $p < 0.001$, cluster-extent threshold: $pFWE < 0.05$) (Fig. 4, Supplementary Table S5). The proportion of voxels within this cluster that overlapped with song network ROIs (5.38%) exceeded that which would be expected by chance (*Mdn* null overlap: 4.84%, 95% CI = [4.80%, 4.87%], $p < 0.0001$).

3.6.1. Voxel-wise homotopic FC is stronger than ipsilateral or heterotopic FC

An LME random intercept model was fit in which average voxel-wise FC served as the criterion variable, and fixed-effects predictors included connection type, age, isoflurane dose, and body temperature; a random intercept was included for bird. The main effect of connection type was significant ($\chi^2(2) = 58.14$, $p < 0.001$). Simple effect contrasts revealed that homotopic FC was significantly stronger than either ipsilateral FC ($B = 1.51$, $t(51) = 8.43$, $p < 0.001$) or heterotopic FC ($B = 1.63$, $t(51) = 9.08$, $p < 0.001$), whereas heterotopic and ipsilateral FC were not significantly different ($B = -0.12$, $t(51) = -0.65$, $p > 0.50$). The voxel-wise distributions of FC for each connection type are displayed in Fig. 5.

3.6.2. Full model for voxel-wise FC

Finally, we replicated the optimal model for predicting ROI FC (section 3.5, Table 1), here using average voxel-wise FC. Euclidean distance

Table 1
Full model including all fixed-effects covariates.

Fixed Effects	Estimate	*SE*	β	*t*	*p*	95% CI
Intercept	0.4868	0.1069	–	4.55	<0.001	[0.277, 0.697]
Homotopic-nSC	0.3851	0.0829	0.93	4.65	<0.001	[0.223, 0.548]
Homotopic-SC	0.6248	0.1005	1.38	6.21	<0.001	[0.428, 0.822]
Ipsilateral	−0.0280	0.0294	−0.13	−0.95	0.340	[-0.086, 0.030]
Age	0.0003	0.0002	0.04	1.55	0.120	[-0.000, 0.001]
Body Temperature	−0.0086	0.0028	−0.06	−3.05	0.002	[-0.014, −0.003]
Isoflurane	−0.0265	0.0122	−0.05	−2.18	0.029	[-0.050, −0.003]
Euclidean Distance	−0.0220	0.0017	−0.21	−12.76	<0.001	[-0.025, −0.019]
ROI Volume	0.0165	0.0015	0.16	10.88	<0.001	[0.014, 0.019]
Homotopic-nSC:Age	0.0003	0.0006	0.04	0.43	0.670	[-0.001, 0.001]
Homotopic-SC:Age	−0.0024	0.0007	−0.36	−3.35	0.001	[-0.004, −0.001]
Ipsilateral:Age	−0.0003	0.0002	−0.04	−1.21	0.227	[-0.001, 0.000]
Homotopic-nSC:Isoflurane	−0.1410	0.0456	−0.28	−3.09	0.002	[-0.230, −0.052]
Homotopic-SC:Isoflurane	−0.1538	0.0552	−0.30	−2.78	0.005	[-0.262, −0.046]
Ipsilateral:Isoflurane	0.0116	0.0161	0.02	0.72	0.473	[-0.020, 0.043]
Random Effects						
Groups	**Name**	**Std. Dev.**		**95% CI**		
Bird	Intercept	0.005		[0.001, 0.023]		
Error	Residual	0.142		[0.139, 0.146]		

Note. *DFE* = 3595, *R*squared = 0.179, Adjusted *R*squared = 0.176.

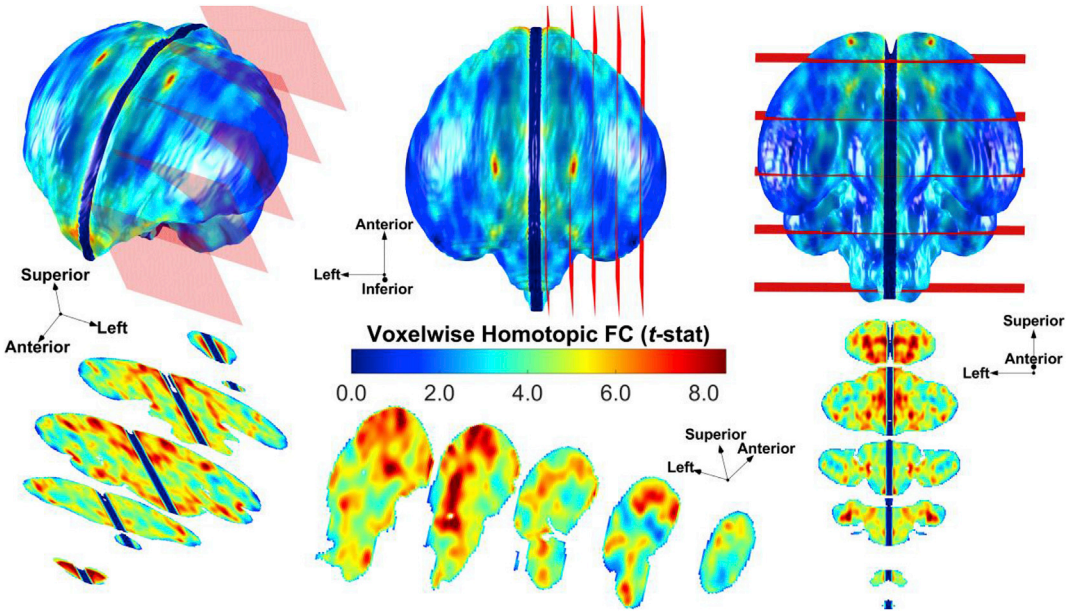

Fig. 4. Zebra finch voxel-mirrored homotopic connectivity (VMHC). *Top row:* three views (*left:* left lateral/anterior diagonal view, *middle:* dorsal view, *right:* posterior view) of a 3D rendering of the zebra finch brain template, with homotopic FC (as *t*-statistics from one-sample tests for homotopic FC across birds and ages) plotted on its surface. Red meshes indicate the location of slices used for the bottom row of plots. *Bottom row*: three slice orientations (*left:* coronal, *middle:* sagittal, *right:* axial) depicting homotopic FC. 3D axes display panel orientation. A single, large significant cluster of homotopic FC was identified, encompassing 87.8% of the total brain volume (primary threshold: $p < 0.001$, cluster-extent threshold: $pFWE < 0.05$; Supplementary Table S5). The color bar [range: 0–8.5] indicates the color-scaling of *t*-statistics.

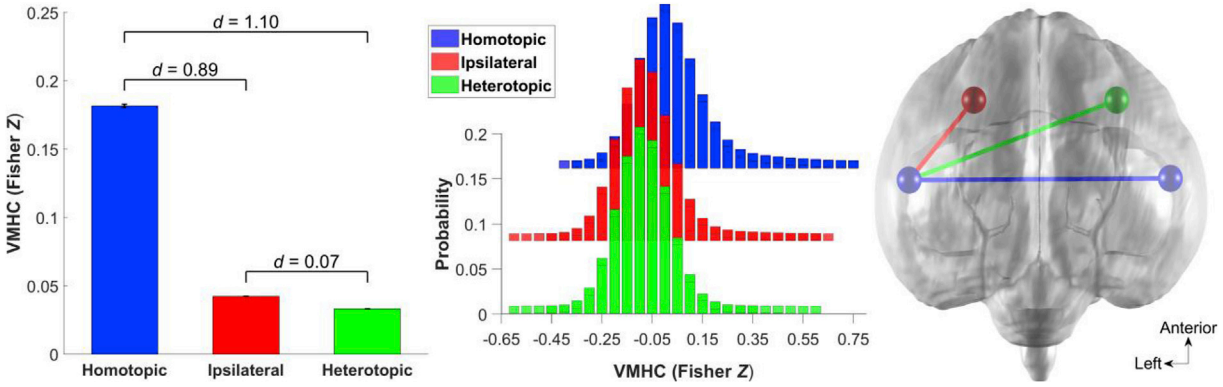

Fig. 5. The relative voxel-mirrored homotopic connectivity (VMHC) strength of different connection types (homotopic, ipsilateral, heterotopic). *Left:* Bar plot showing mean voxel-wise FC values as Fisher *Z*-transformed Pearson correlations apportioned by connection type. Error-bars represent 95% confidence intervals, and Cohen's *d* effect sizes are displayed above each connection type contrast. *Middle:* Histograms showing the distribution of FC values for each connection type. Histogram bins were normalized as the probability of FC of a given magnitude for each connection type. *Right:* A schematic illustrating each connection type overlaid on a superior view of the zebra finch brain template. Axes show brain orientation.

and ROI volume were ROI-specific measures, and they could not be controlled for in this case, given that the criterion variable here was average voxel-wise FC across the whole brain. We therefore implemented an LME random intercept model which included all of the following fixed-effects covariates: (1) connection type (homotopic, ipsilateral, heterotopic), (2) age, (3) body temperature, (4) isoflurane dose, (5) a connection type by age interaction, and (6) a connection type by isoflurane dose interaction. Additionally, a random intercept was included for bird. We then proceeded to reduce the model by minimizing AIC, assuring that nested models were significantly different based on likelihood-ratio drop-tests: (1) the age by connection type interaction was not significant ($\chi^2(2) = 1.00$, $p > 0.60$) and was dropped ($\Delta AIC = 3.00$; Burnham and Anderson, 2004); (2) the main effect of age was not significant ($B = 0.003$, $t(49) = 0.88$, $p > 0.35$) and was dropped ($\Delta AIC = 1.23$). The model was not further reducible based on AIC (i.e., dropping additional predictors yielded higher AIC), thus yielding the final model displayed in Table 2 below.

Consistent with ROI-based analyses, homotopic FC was significantly stronger than heterotopic FC ($B = 4.92$, $t(50) = 5.34$, $p < 0.001$), whereas ipsilateral and heterotopic FC were not significantly different ($B = 0.15$, $t(50) = 0.16$, $p > 0.85$). Also consistent with ROI-based analyses, we noted a significant isoflurane dose by connection type interaction ($\chi^2(2) = 14.99$, $p < 0.001$), such that higher isoflurane dose was associated with selectively reduced homotopic FC, relative to heterotopic FC ($B = -1.83$, $t(50) = -3.63$, $p < 0.001$). In contrast, ipsilateral and heterotopic FC did not significantly differ based on isoflurane dose ($B = -0.017$, $t(50) = -0.03$, $p > 0.90$).

Table 2
Voxel-wise FC model.

Fixed Effects	Estimate	*SE*	*β*	*T*	*p*	95% CI
Intercept	8.8938	2.5355	–	3.51	0.001	[3.801, 13.986]
Ipsilateral	0.1468	0.9205	0.12	0.16	0.874	[-1.702, 1.996]
Homotopic	4.9166	0.9205	1.63	5.34	<0.001	[3.068, 6.765]
Isoflurane	0.1373	0.3750	0.04	0.37	0.716	[-0.616, 0.890]
Body Temperature	−0.2401	0.0648	−0.27	−3.71	0.001	[-0.370, −0.110]
Ipsilateral:Isoflurane	−0.0168	0.5054	−0.01	−0.03	0.974	[-1.032, 0.998]
Homotopic:Isoflurane	−1.8330	0.5054	−0.57	−3.63	0.001	[-2.848, −0.818]
Random Effects						
Groups	**Name**	**Std. Dev.**		**95% CI**		
Bird	Intercept	0.111		[0.021, 0.599]		
Error	Residual	0.480		[0.369, 0.582]		

Note. *DFE* = 50, *R*squared = 0.769, Adjusted *R*squared = 0.742.

4. Discussion

To our knowledge, these results provide the first indication of widespread homotopic FC in a non-Eutherian brain at rest. Non-invasive rs-fMRI enabled us to obtain repeated measures across development from the same intact zebra finches, and allowed us to conduct voxel-wise analyses to examine the spatial distribution of homotopic FC across the entire zebra finch brain. We noted robust homotopic FC throughout a brain network necessary for learned song, and follow-up analyses revealed that, consistent with Eutherian brain connectivity (Honey et al., 2009; Shen et al., 2015), homotopic FC was stronger between regions that also shared homotopic SC. Also, consistent with the developmental increases in lateralization observed in humans from childhood through middle adulthood (Zuo et al., 2010), we found that homotopic FC decreased across development in the zebra finch brain, but this result appeared to be specific to homotopic-SC connections. Beyond extending the finding of homotopic FC across phylogeny, the present results also underline the efficacy of rs-fMRI paradigms for investigating both comparative neuroscience questions and vocal learning in songbirds. The ability to conduct longitudinal investigations during a short sensitive period for vocal development makes the zebra finch an ideal model organism for such investigations.

VMHC analyses revealed that homotopic FC is a brain-wide phenomenon in the zebra finch, apparent even when examined without *a priori* defined ROIs. Interestingly, the voxel-wise distribution of homotopic FC exhibited an apparent medial bias, notably similar to the voxel-wise pattern observed in the human brain (Stark et al., 2008; Zuo et al., 2010). Importantly, the midline homotopic FC observed here was not an artefact of spatial smoothing, as we discarded data within a four-voxel radius of the midline before proceeding to data analyses. Although homotopic FC appeared widely distributed, we also found that the song network exhibited greater spatial overlap with the significant voxel-wise homotopic FC cluster than expected by chance. This provides an initial suggestion that bilateral coordination may be of particular functional importance for song, a complex and distributed multimodal brain process. Future studies will benefit from the incorporation of song data to further test this intriguing possibility.

Notably, we failed to find evidence to suggest that the FC of subtelencephalic homotopic-SC connections mediated song network homotopic FC. We examined a well-characterized circuit that links bilateral HVC, relying critically on Uva of the thalamus (Schmidt et al., 2006; Ashmore et al., 2008). Although this circuit did not appear to mediate the homotopic FC observed between bilateral HVC, as measured in terms of intrinsic brain activity, evidence suggests that it likely *does* mediate interhemispheric premotor coordination during vocalization (Schmidt et al., 2006; Ashmore et al., 2008). Thus, it is possible that this pathway represents a task-specific structural mechanism for interhemispheric coordination, as opposed to a more domain-general SC pathway for mediating widespread intrinsic homotopic FC such as that observed here in the resting-state. It is also possible that interhemispheric coordination via Uva SC occurs on a timescale not detectable via rs-fMRI measurements of infra-slow brain activity. However, evidence does suggest that synchronization in the amplitude envelope fluctuations of much faster signals (e.g., Gamma) can be detected by rs-fMRI (Mantini et al., 2007; He et al., 2008; Sadaghiani et al., 2010; Ko et al., 2011; Hacker et al., 2017). In light of these results, an informative topic for future studies would be to investigate additional sub-telencephalic SC pathways that might underlie domain-general interhemispheric coordination of intrinsic, as opposed to task-related, brain activity. For instance, future studies might further explore the role played by the indirect SC of the AC, perhaps with the aid of diffusion imaging (Hamaide et al., 2017).

Interestingly, the reliance of homotopic FC on the CC in Eutherian mammals appears to be somewhat region specific (Paul et al., 2007; O'Reilly et al., 2013; Roland et al., 2017) and resilient to structural insults (Uddin et al., 2008; Khanna et al., 2012; O'Reilly et al., 2013), leading to the suggestion that dual structural mechanisms may underlie homotopic FC in these organisms: (1) a cortical mechanism relying on interhemispheric transfer via the CC, and (2) a subcortical mechanism relying on interhemispheric structural projections between sub-telencephalic regions such as the thalamus, midbrain, brainstem, and/or other subcortical nuclei (Uddin et al., 2008). It has been posited that the former mechanism predominates in normal ontogeny, but that the latter mechanism may compensate in cases of loss or damage of the CC by retaining the transfer of simpler, often unimodal information (Glickstein and Sperry, 1960; Glickstein et al., 1998; Paul et al., 2007; Uddin et al., 2008; Glickstein, 2009). The present results, in an organism that lacks the CC in normal ontogeny, suggest the possibility that the largely heterotopic and much less extensive avian AC (Letzner et al., 2016) may be sufficient for mediating widespread homotopic FC via indirect SC. It is notable that we not only observed robust homotopic FC in the zebra finch brain between primary sensory regions such as Field L, which might be predicted from studies of CC dysgenesis, but also between higher-level processing areas such as the auditory forebrain (here, NCM and CM), among others.

In addition to interhemispheric communication via SC, other potential mechanisms underlying homotopic FC have also been proposed, including 1. brain activity driven by symmetric sensory inputs (Van Essen, 2005; Shen et al., 2015) and 2. neuromodulation by bilaterally symmetric ascending arousal systems (e.g., acetylcholine; Ryan and Arnold, 1981; Sakaguchi and Saito, 1989; Everitt and Robbins, 1997; Shen et al., 2015; Turchi et al., 2018). The first hypothetical mechanism appears unlikely to underlie homotopic FC in the present study, given that homotopic FC was widespread throughout the brain and not limited to primary sensory regions. Additionally, while registration of sensory input does still occur in songbirds under anesthesia (Van Meir et al.,

2005; Boumans et al., 2007), the zebra finches' eyes were closed during scanning, limiting visual input, and foam earplugs were provided to limit scanner noise and auditory input. Although these precautions likely did not eliminate the potential for symmetric sensory input driving brain activity, they at least helped to mitigate this potential.

Although the second hypothetical mechanism is an interesting possibility, a recent study in macaques found that inactivation of ascending arousal systems in one hemisphere leads to a drop in fMRI signal amplitude ipsilaterally, but it does not appear to abolish homotopic FC, nor does it significantly change the shape of well-known resting-state networks (Turchi et al., 2018). These results do not support the notion that ascending arousal systems are critical for homotopic FC in Eutherian mammals. Regardless of which specific mechanism (or combination of mechanisms) underlies homotopic FC in non-Eutherian vertebrates, the zebra finch, which lacks the CC in normal ontogeny, and which presumably also lacks any compensatory structural plasticity observed in callosal dysgenesis (Tovar-Moll et al., 2014), provides an ideal model organism for investigating the role of alternative mechanisms to direct SC that may also contribute to interhemispheric coordination.

Notably, we designed our scanning paradigm to utilize a light dose of isoflurane anesthesia based on prior work demonstrating the validity of this procedure for zebra finch fMRI (e.g., Boumans et al., 2007; Poirier et al., 2009, 2010). Prior work in mammals has found that isoflurane reduces the magnitude of hemodynamic responses, but their shape remains similar to that of awake animals (Shtoyerman et al., 2000; Fukuda et al., 2005; Zhao et al., 2007). A number of studies in humans (Greicius et al., 2003; Boveroux et al., 2010; Martuzzi et al., 2010) and macaques (Vincent et al., 2007) have also found that prominent resting-state networks, including the default-mode network, are preserved under a variety of anesthetics, although often with somewhat reduced correlations. Notably, a recent study directly compared BOLD responses to auditory stimuli in awake versus isoflurane anesthetized zebra finches (Van Ruijssevelt et al., 2017). This study found no difference in the magnitude of auditory-evoked BOLD responses, nor differences in neural selectivity for natural versus synthetic sounds, between awake versus isoflurane anesthetized birds; in contrast, the spatial extent of activation was slightly larger under isoflurane (Van Ruijssevelt et al., 2017). This study raises the possibility of confirming the presence of homotopic FC in awake zebra finches in future studies. As noted previously, recent evidence from rodents indicates that an increase in isoflurane dose from 1% to 2% is associated with a concomitant decrease in homotopic FC (Hutchison et al., 2014; Bukhari et al., 2018), and here we also found that higher isoflurane doses predicted selectively lower homotopic FC in zebra finches. If this trend also holds for lower doses of isoflurane, this predicts that awake zebra finches should exhibit greater homotopic FC than anesthetized zebra finches, an interesting possibility to be explored in future studies.

Although the present study is unique as a longitudinal whole-brain rs-fMRI investigation in zebra finches, it was the beneficiary of a growing body of literature focused on the neuroimaging of songbirds (e.g., Boumans et al., 2007; Poirier et al., 2009, 2010; Poirier and Van der Linden, 2011; Van Ruijssevelt et al., 2017). For instance, we utilized a spin-echo fMRI sequence, as opposed to gradient echo, to avoid susceptibility artefacts previously shown to be more prevalent in songbirds (Poirier and Van der Linden, 2011). In addition to these precautions, we applied a bandpass filter to remove high frequency components of cardiac and respiratory contributions to the signal (>0.10 Hz Biswal et al., 1996; Murphy et al., 2013), regressed out principal components of CSF signals to further remove physiological noise (Behzadi et al., 2007), and assured the quality of our resting-state signals using *tSNR* and power spectral analyses. We also measured and controlled for effects of Euclidean distance between ROIs, ROI volume, and body temperature. Even with these rigorous statistical controls, we still observed robust homotopic FC across much of the zebra finch brain, supporting a biological, rather than technical or artefactual, origin for these findings.

5. Conclusion

In sum, our results indicate that a homotopic functional brain architecture likely arose in animals prior to the evolution of the CC, suggesting that this marker of interhemispheric coordination may be a neural feature observed more broadly across phylogeny, beyond the Eutherian mammals. Accordingly, rather than serving as a necessary prerequisite for homotopic FC, the CC may have evolved to provide finer dynamic control over, or flexible switching between, bilateral coordination and hemispheric specialization (Aboitiz and Montiel, 2003; van der Knaap and van der Ham, 2011). Such insights, in conjunction with the present results, increase the plausibility of the notion that ancestral pathways such as the AC (Paterson and Bottjer, 2017) or symmetric ascending bilateral inputs (Ashmore et al., 2008) are sufficient to provide the balance of interhemispheric coordination and specialization required for complex multimodal cognition in non-Eutherian vertebrates. Future studies are merited to investigate links between homotopic FC in non-mammalian vertebrates and complex brain functions requiring hemispheric specialization and coordination, such as song learning.

Conflicts of interest

No competing interests declared.

Acknowledgements

We thank the staff of the MRIS facility, Xiaobing Fan, and Frank Ibarra for their technical assistance, and Elisa Gores for bird care. This work was supported by a grant from the Big Ideas Generator at the University of Chicago, awarded to SEL and MGB, and a National Science Foundation grant (BCS-1632445), awarded to MGB.

Appendix A. Supplementary data

Supplementary data to this article can be found online at https://doi.org/10.1016/j.neuroimage.2019.03.064.

References

Aboitiz, F., Montiel, J., 2003. One hundred million years of interhemispheric communication: the history of the corpus callosum. Braz. J. Med. Biol. Res. 36, 409–420.
Aronov, D., Andalman, A.S., Fee, M.S., 2008. A specialized forebrain circuit for vocal babbling in the juvenile songbird. Science 320, 630–634.
Ashmore, R.C., Bourjaily, M., Schmidt, M.F., 2008. Hemispheric coordination is necessary for song production in adult birds: implications for a dual role for forebrain nuclei in vocal motor control. J. Neurophysiol. 99, 373–385.
Avants, B.B., Tustison, N., Song, G., 2009. Advanced normalization tools (ANTS). Insight J 2, 1–35.
Avants, B.B., Tustison, N.J., Song, G., Cook, P.A., Klein, A., Gee, J.C., 2011. A reproducible evaluation of ANTs similarity metric performance in brain image registration. Neuroimage 54, 2033–2044.
Avants, B.B., Yushkevich, P., Pluta, J., Minkoff, D., Korczykowski, M., Detre, J., Gee, J.C., 2010. The optimal template effect in hippocampus studies of diseased populations. Neuroimage 49, 2457–2466.
Avey, M.T., Phillmore, L.S., MacDougall-Shackleton, S.A., 2005. Immediate early gene expression following exposure to acoustic and visual components of courtship in zebra finches. Behav. Brain Res. 165, 247–253.
Barth, M., Norris, D.G., 2007. Very high-resolution three-dimensional functional MRI of the human visual cortex with elimination of large venous vessels. NMR Biomed. 20, 477–484.
Behzadi, Y., Restom, K., Liau, J., Liu, T.T., 2007. A component based noise correction method (CompCor) for BOLD and perfusion based fMRI. Neuroimage 37, 90–101.
Biswal, B., Deyoe, E.A., Hyde, J.S., 1996. Reduction of physiological fluctuations in fMRI using digital filters. Magn. Reson. Med. 35, 107–113.
Biswal, B., Yetkin, F.Z., Haughton, V.M., Hyde, J.S., 1995. Functional connectivity in the motor cortex of resting human brain using echo-planar mri. Magn. Reson. Med. 34, 537–541.
Biswal, B.B., Mennes, M., Zuo, X.-N., Gohel, S., Kelly, C., Smith, S.M., Beckmann, C.F., Adelstein, J.S., Buckner, R.L., Colcombe, S., Dogonowski, A.-M., Ernst, M., Fair, D., Hampson, M., Hoptman, M.J., Hyde, J.S., Kiviniemi, V.J., Kötter, R., Li, S.-J., Lin, C.-P., Lowe, M.J., Mackay, C., Madden, D.J., Madsen, K.H., Margulies, D.S., Mayberg, H.S., McMahon, K., Monk, C.S., Mostofsky, S.H., Nagel, B.J., Pekar, J.J., Peltier, S.J., Petersen, S.E., Riedl, V., Rombouts, S.A.R.B., Rypma, B., Schlaggar, B.L.,

Schmidt, S., Seidler, R.D., Siegle, G.J., Sorg, C., Teng, G.-J., Veijola, J., Villringer, A., Walter, M., Wang, L., Weng, X.-C., Whitfield-Gabrieli, S., Williamson, P., Windischberger, C., Zang, Y.-F., Zhang, H.-Y., Castellanos, F.X., Milham, M.P., 2010. Toward discovery science of human brain function. Proc. Natl. Acad. Sci. Unit. States Am. 107, 4734–4739.

Boumans, T., Theunissen, F.E., Poirier, C., Van Der Linden, A., 2007. Neural representation of spectral and temporal features of song in the auditory forebrain of zebra finches as revealed by functional MRI. Eur. J. Neurosci. 26, 2613–2626.

Boveroux, P., Vanhaudenhuyse, A., Bruno, M.-A., Noirhomme, Q., Lauwick, S., Luxen, A., Degueldre, C., Plenevaux, A., Schnakers, C., Phillips, C., Brichant, J.-F., Bonhomme, V., Maquet, P., Greicius, M.D., Laureys, S., Boly, M., 2010. Breakdown of within- and between-network resting state functional magnetic resonance imaging connectivity during propofol-induced loss of consciousness. Anesthesiol. J. Am. Soc. Anesthesiol. 113, 1038–1053.

Bright, M.G., Murphy, K., 2015. Is fMRI "noise" really noise? Resting state nuisance regressors remove variance with network structure. Neuroimage 114, 158–169.

Budde, J., Shajan, G., Zaitsev, M., Scheffler, K., Pohmann, R., 2014. Functional MRI in human subjects with gradient-echo and spin-echo EPI at 9.4 T. Magn. Reson. Med. 71, 209–218.

Bukhari, Q., Schroeter, A., Rudin, M., 2018. Increasing isoflurane dose reduces homotopic correlation and functional segregation of brain networks in mice as revealed by resting-state fMRI. Sci. Rep. 8, 10591.

Burnham, K.P., Anderson, D.R., 2004. Multimodel inference: understanding AIC and BIC in model selection. Socio. Methods Res. 33, 261–304.

Casimo, K., Grassia, F., Poliachik, S.L., Novotny, E., Poliakov, A., Ojemann, J.G., 2018. Preservation of electrophysiological functional connectivity after partial corpus callosotomy: case report. J. Neurosurg. Pediatr. 22, 214–219.

Chang, W.-T., Puspitasari, F., Garcia-Miralles, M., Yeow, L.Y., Tay, H.-C., Koh, K.B., Tan, L.J., Pouladi, M.A., Chuang, K.-H., 2018. Connectomic imaging reveals Huntington-related pathological and pharmaceutical effects in a mouse model. NMR Biomed. 31, e4007.

Cordes, D., Haughton, V.M., Arfanakis, K., Carew, J.D., Turski, P.A., Moritz, C.H., Quigley, M.A., Meyerand, M.E., 2001. Frequencies contributing to functional connectivity in the cerebral cortex in "resting-state" data. Am. J. Neuroradiol. 22, 1326–1333.

Cynx, J., Williams, H., Nottebohm, F., 1992. Hemispheric differences in avian song discrimination. Proc. Natl. Acad. Sci. Unit. States Am. 89, 1372–1375.

De Groof, G., Verhoye, M., Van Meir, V., Tindemans, I., Leemans, A., Van der Linden, A., 2006. In vivo diffusion tensor imaging (DTI) of brain subdivisions and vocal pathways in songbirds. Neuroimage 29, 754–763.

Desai, M., Kahn, I., Knoblich, U., Bernstein, J., Atallah, H., Yang, A., Kopell, N., Buckner, R.L., Graybiel, A.M., Moore, C.I., Boyden, E.S., 2010. Mapping brain networks in awake mice using combined optical neural control and fMRI. J. Neurophysiol. 105, 1393–1405.

Doupe, A.J., Kuhl, P.K., 1999. Birdsong and human speech: common themes and mechanisms. Annu. Rev. Neurosci. 22, 567–631.

Duff, E.P., Johnston, L.A., Xiong, J., Fox, P.T., Mareels, I., Egan, G.F., 2008. The power of spectral density analysis for mapping endogenous BOLD signal fluctuations. Hum. Brain Mapp. 29, 778–790.

Eklund, A., Nichols, T.E., Knutsson, H., 2016. Cluster failure: why fMRI inferences for spatial extent have inflated false-positive rates. Proc. Natl. Acad. Sci. Unit. States Am. 113 (28), 7900–7905 .

Everitt, B.J., Robbins, T.W., 1997. Central cholinergic systems and cognition. Annu. Rev. Psychol. 48, 649–684.

Fukuda, M., Rajagopalan, U.M., Homma, R., Matsumoto, M., Nishizaki, M., Tanifuji, M., 2005. Localization of activity-dependent changes in blood volume to submillimeter-scale functional domains in cat visual cortex. Cerebr. Cortex 15, 823–833.

Galvis, D., Wu, W., Hyson, R.L., Johnson, F., Bertram, R., 2018. Interhemispheric dominance switching in a neural network model for birdsong. J. Neurophysiol. 120, 1186–1197.

Gazzaniga, M.S., 2000. Cerebral specialization and interhemispheric communication: does the corpus callosum enable the human condition? Brain 123, 1293–1326.

Geschwind, N., 1970. The organization of language and the brain. Science 170, 940–944.

Glickstein, M., 2009. Paradoxical inter-hemispheric transfer after section of the cerebral commissures. Exp. Brain Res. 192, 425.

Glickstein, M., Buchbinder, S., Iii, J.L.M., 1998. Visual control of the arm, the wrist and the fingers: pathways through the brain. Neuropsychologia 36, 981–1001.

Glickstein, M., Sperry, R.W., 1960. Intermanual somesthetic transfer in split-brain rhesus monkeys. J. Comp. Physiol. Psychol. 53, 322–327.

Grandjean, J., Schroeter, A., Batata, I., Rudin, M., 2014. Optimization of anesthesia protocol for resting-state fMRI in mice based on differential effects of anesthetics on functional connectivity patterns. Neuroimage 102, 838–847.

Greicius, M.D., Krasnow, B., Reiss, A.L., Menon, V., 2003. Functional connectivity in the resting brain: a network analysis of the default mode hypothesis. Proc. Natl. Acad. Sci. Unit. States Am. 100, 253–258.

Hacker, C.D., Snyder, A.Z., Pahwa, M., Corbetta, M., Leuthardt, E.C., 2017. Frequency-specific electrophysiologic correlates of resting state fMRI networks. Neuroimage 149, 446–457.

Hallquist, M.N., Hwang, K., Luna, B., 2013. The nuisance of nuisance regression: spectral misspecification in a common approach to resting-state fMRI preprocessing reintroduces noise and obscures functional connectivity. Neuroimage 82, 208–225.

Hamaguchi, K., Tanaka, M., Mooney, R., 2016. A distributed recurrent network contributes to temporally precise vocalizations. Neuron 91, 680–693.

Hamaide, J., De Groof, G., Van Steenkiste, G., Jeurissen, B., Van Audekerke, J., Naeyaert, M., Van Ruijssevelt, L., Cornil, C., Sijbers, J., Verhoye, M., 2017. Exploring sex differences in the adult zebra finch brain: in vivo diffusion tensor imaging and ex vivo super-resolution track density imaging. Neuroimage 146, 789–803.

Harmer, J., Sanchez-Panchuelo, R.M., Bowtell, R., Francis, S.T., 2012. Spatial location and strength of BOLD activation in high-spatial-resolution fMRI of the motor cortex: a comparison of spin echo and gradient echo fMRI at 7 T. NMR Biomed. 25, 717–725.

He, B.J., Snyder, A.Z., Zempel, J.M., Smyth, M.D., Raichle, M.E., 2008. Electrophysiological correlates of the brain's intrinsic large-scale functional architecture. Proc. Natl. Acad. Sci. Unit. States Am. 105, 16039–16044.

Heath, C.J., Jones, E.G., 1971. Interhemispheric pathways in the absence of a corpus callosum. An experimental study of commissural connexions in the marsupial phalanger. J. Anat. 109, 253–270.

Hermesdorf, M., Sundermann, B., Feder, S., Schwindt, W., Minnerup, J., Arolt, V., Berger, K., Pfleiderer, B., Wersching, H., 2016. Major depressive disorder: findings of reduced homotopic connectivity and investigation of underlying structural mechanisms. Hum. Brain Mapp. 37, 1209–1217.

Honey, C.J., Sporns, O., Cammoun, L., Gigandet, X., Thiran, J.-P., Meuli, R., Hagmann, P., 2009. Predicting human resting-state functional connectivity from structural connectivity. Proc. Natl. Acad. Sci. Unit. States Am. 106, 2035–2040.

Huber, L., Tse, D.H.Y., Wiggins, C.J., Uludağ, K., Kashyap, S., Jangraw, D.C., Bandettini, P.A., Poser, B.A., Ivanov, D., 2018. Ultra-high resolution blood volume fMRI and BOLD fMRI in humans at 9.4 T: Capabilities and challenges. Neuroimage 178, 769–779.

Hutchison, R.M., Hutchison, M., Manning, K.Y., Menon, R.S., Everling, S., 2014. Isoflurane induces dose-dependent alterations in the cortical connectivity profiles and dynamic properties of the brain's functional architecture. Hum. Brain Mapp. 35, 5754–5775.

Hutton, C., Josephs, O., Stadler, J., Featherstone, E., Reid, A., Speck, O., Bernarding, J., Weiskopf, N., 2011. The impact of physiological noise correction on fMRI at 7T. Neuroimage 57, 101–112.

Jarbo, K., Verstynen, T., Schneider, W., 2012. In vivo quantification of global connectivity in the human corpus callosum. Neuroimage 59, 1988–1996.

Jin, T., Wang, P., Tasker, M., Zhao, F., Kim, S.-G., 2006. Source of nonlinearity in echo-time-dependent BOLD fMRI. Magn. Reson. Med. 55, 1281–1290.

Johnston, J.M., Vaishnavi, S.N., Smyth, M.D., Zhang, D., He, B.J., Zempel, J.M., Shimony, J.S., Snyder, A.Z., Raichle, M.E., 2008. Loss of resting interhemispheric functional connectivity after complete section of the corpus callosum. J. Neurosci. 28, 6453–6458.

Johnstone, T., Ores Walsh, K.S., Greischar, L.L., Alexander, A.L., Fox, A.S., Davidson, R.J., Oakes, T.R., 2006. Motion correction and the use of motion covariates in multiple-subject fMRI analysis. Hum. Brain Mapp. 27, 779–788.

Kalthoff, D., Seehafer, J.U., Po, C., Wiedermann, D., Hoehn, M., 2011. Functional connectivity in the rat at 11.7 T: Impact of physiological noise in resting state fMRI. Neuroimage 54, 2828–2839.

Kannurpatti, S.S., Biswal, B.B., Kim, Y.R., Rosen, B.R., 2008. Spatio-temporal characteristics of low-frequency BOLD signal fluctuations in isoflurane-anesthetized rat brain. Neuroimage 40, 1738–1747.

Kelly, C., Zuo, X.-N., Gotimer, K., Cox, C.L., Lynch, L., Brock, D., Imperati, D., Garavan, H., Rotrosen, J., Castellanos, F.X., 2011. Reduced interhemispheric resting state functional connectivity in cocaine addiction. Biol. Psychiatry 69, 684–692.

Kemper, V.G., De Martino, F., Vu, A.T., Poser, B.A., Feinberg, D.A., Goebel, R., Yacoub, E., 2015. Sub-millimeter T2 weighted fMRI at 7 T: comparison of 3D-GRASE and 2D SE-EPI. Front. Neurosci. 9.

Khanna, P.C., Poliakov, A.V., Ishak, G.E., Poliachik, S.L., Friedman, S.D., Saneto, R.P., Novotny, E.J., Ojemann, J.G., Shaw, D.W.W., 2012. Preserved interhemispheric functional connectivity in a case of corpus callosum agenesis. Neuroradiology 54, 177–179.

Kim, J., Van Dijk, K.R., Libby, A., Napadow, V., 2014. Frequency-dependent relationship between resting-state functional magnetic resonance imaging signal power and head motion is localized within distributed association networks. Brain Connect. 4, 30–39.

Ko, A.L., Darvas, F., Poliakov, A., Ojemann, J., Sorensen, L.B., 2011. Quasi-periodic fluctuations in default mode network electrophysiology. J. Neurosci. 31, 11728–11732.

Layden, E.A., Cacioppo, J.T., Cacioppo, S., Cappa, S.F., Dodich, A., Falini, A., Canessa, N., 2017. Perceived social isolation is associated with altered functional connectivity in neural networks associated with tonic alertness and executive control. Neuroimage 145, 58–73.

Lee, S.-P., Silva, A.C., Ugurbil, K., Kim, S.-G., 1999. Diffusion-weighted spin-echo fMRI at 9.4 T: Microvascular/tissue contribution to BOLD signal changes. Magn. Reson. Med. 42, 919–928.

Letzner, S., Simon, A., Güntürkün, O., 2016. Connectivity and neurochemistry of the commissura anterior of the pigeon (Columba livia). J. Comp. Neurol. 524, 343–361.

Liska, A., Galbusera, A., Schwarz, A.J., Gozzi, A., 2015. Functional connectivity hubs of the mouse brain. Neuroimage 115, 281–291.

Lu, J., Liu, H., Zhang, M., Wang, D., Cao, Y., Ma, Q., Rong, D., Wang, X., Buckner, R.L., Li, K., 2011. Focal pontine lesions provide evidence that intrinsic functional connectivity reflects polysynaptic anatomical pathways. J. Neurosci. 31, 15065–15071.

Luo, Z.-X., Yuan, C.-X., Meng, Q.-J., Ji, Q., 2011. A Jurassic eutherian mammal and divergence of marsupials and placentals. Nature 476, 442–445.

Mantini, D., Perrucci, M.G., Gratta, C.D., Romani, G.L., Corbetta, M., 2007. Electrophysiological signatures of resting state networks in the human brain. Proc. Natl. Acad. Sci. Unit. States Am. 104, 13170–13175.

Martuzzi, R., Ramani, R., Qiu, M., Rajeevan, N., Constable, R.T., 2010. Functional connectivity and alterations in baseline brain state in humans. Neuroimage 49, 823–834.

Matsui, T., Murakami, T., Ohki, K., 2016. Transient neuronal coactivations embedded in globally propagating waves underlie resting-state functional connectivity. Proc. Natl. Acad. Sci. Unit. States Am. 113, 6556–6561.
Mikl, M., Mareček, R., Hluštík, P., Pavlicová, M., Drastich, A., Chlebus, P., Brázdil, M., Krupa, P., 2008. Effects of spatial smoothing on fMRI group inferences. Magn. Reson. Imaging 26, 490–503.
Mišić, B., Fatima, Z., Askren, M.K., Buschkuehl, M., Churchill, N., Cimprich, B., Deldin, P.J., Jaeggi, S., Jung, M., Korostil, M., 2014. The functional connectivity landscape of the human brain. PLoS One 9, e111007.
Mitra, A., Kraft, A., Wright, P., Acland, B., Snyder, A.Z., Rosenthal, Z., Czerniewski, L., Bauer, A., Snyder, L., Culver, J., Lee, J.-M., Raichle, M.E., 2018. Spontaneous infra-slow brain activity has unique spatiotemporal dynamics and laminar structure. Neuron 98, 297–305 e6.
Molloy, E.K., Meyerand, M.E., Birn, R.M., 2014. The influence of spatial resolution and smoothing on the detectability of resting-state and task fMRI. Neuroimage 86, 221–230.
Mooney, R., Rao, M., 1994. Waiting periods versus early innervation: the development of axonal connections in the zebra finch song system. J. Neurosci. 14, 6532–6543.
Moorman, S., Gobes, S.M., Kuijpers, M., Kerkhofs, A., Zandbergen, M.A., Bolhuis, J.J., 2012. Human-like brain hemispheric dominance in birdsong learning. Proc. Natl. Acad. Sci. Unit. States Am. 109, 12782–12787.
Moorman, S., Gobes, S.M.H., van de Kamp, F.C., Zandbergen, M.A., Bolhuis, J.J., 2015. Learning-related brain hemispheric dominance in sleeping songbirds. Sci. Rep. 5, 9041.
Murphy, K., Birn, R.M., Bandettini, P.A., 2013. Resting-state fMRI confounds and cleanup. Neuroimage, Mapp. Connectome 80, 349–359.
Murphy, K., Bodurka, J., Bandettini, P.A., 2007. How long to scan? The relationship between fMRI temporal signal to noise ratio and necessary scan duration. Neuroimage 34, 565–574.
O'Reilly, J.X., Croxson, P.L., Jbabdi, S., Sallet, J., Noonan, M.P., Mars, R.B., Browning, P.G.F., Wilson, C.R.E., Mitchell, A.S., Miller, K.L., Rushworth, M.F.S., Baxter, M.G., 2013. Causal effect of disconnection lesions on interhemispheric functional connectivity in rhesus monkeys. Proc. Natl. Acad. Sci. Unit. States Am. 110, 13982–13987.
Pan, W.-J., Thompson, G., Magnuson, M., Majeed, W., Jaeger, D., Keilholz, S., 2011. Broadband local field potentials correlate with spontaneous fluctuations in functional magnetic resonance imaging signals in the rat somatosensory cortex under isoflurane anesthesia. Brain Connect. 1, 119–131.
Paterson, A.K., Bottjer, S.W., 2017. Cortical inter-hemispheric circuits for multimodal vocal learning in songbirds. J. Comp. Neurol.
Paul, L.K., Brown, W.S., Adolphs, R., Tyszka, J.M., Richards, L.J., Mukherjee, P., Sherr, E.H., 2007. Agenesis of the corpus callosum: genetic, developmental and functional aspects of connectivity. Nat. Rev. Neurosci. 8, 287.
Penny, W.D., Friston, K.J., Ashburner, J.T., Kiebel, S.J., Nichols, T.E., 2011. Statistical Parametric Mapping: the Analysis of Functional Brain Images. Academic press.
Poirier, C., Boumans, T., Verhoye, M., Balthazart, J., Van der Linden, A., 2009. Own-song recognition in the songbird auditory pathway: selectivity and lateralization. J. Neurosci. 29, 2252–2258.
Poirier, C., Van der Linden, A.-M., 2011. Spin echo BOLD fMRI on songbirds. Vivo NMR Imag. Methods Protoc. 569–576.
Poirier, C., Vellema, M., Verhoye, M., Van Meir, V., Wild, J.M., Balthazart, J., Van Der Linden, A., 2008. A three-dimensional MRI atlas of the zebra finch brain in stereotaxic coordinates. Neuroimage 41, 1–6.
Poirier, C., Verhoye, M., Boumans, T., Linden, AV der, 2010. Implementation of spin-echo blood oxygen level-dependent (BOLD) functional MRI in birds. NMR Biomed. 23, 1027–1032.
Quigley, M., Cordes, D., Turski, P., Moritz, C., Haughton, V., Seth, R., Meyerand, M.E., 2003. Role of the corpus callosum in functional connectivity. Am. J. Neuroradiol. 24, 208–212.
Roland, J.L., Snyder, A.Z., Hacker, C.D., Mitra, A., Shimony, J.S., Limbrick, D.D., Raichle, M.E., Smyth, M.D., Leuthardt, E.C., 2017. On the role of the corpus callosum in interhemispheric functional connectivity in humans. Proc. Natl. Acad. Sci. Unit. States Am. 114, 13278–13283.
Rua, C., Costagli, M., Symms, M.R., Biagi, L., Donatelli, G., Cosottini, M., Del Guerra, A., Tosetti, M., 2017. Characterization of high-resolution Gradient Echo and Spin Echo EPI for fMRI in the human visual cortex at 7T. Magn. Reson. Imaging 40, 98–108.
Ryan, S.M., Arnold, A.P., 1981. Evidence for cholinergic participation in the control of bird song: acetylcholinesterase distribution and muscarinic receptor autoradiography in the zebra finch brain. J. Comp. Neurol. 202, 211–219.
Sadaghiani, S., Scheeringa, R., Lehongre, K., Morillon, B., Giraud, A.-L., Kleinschmidt, A., 2010. Intrinsic connectivity networks, alpha oscillations, and tonic alertness: a simultaneous electroencephalography/functional magnetic resonance imaging study. J. Neurosci. 30, 10243–10250.
Sakaguchi, H., Saito, N., 1989. The acetylcholine and catecholamine contents in song control nuclei of zebra finch during song ontogeny. Dev. Brain Res. 47, 313–317.
Salvador, R., Martinez, A., Pomarol-Clotet, E., Gomar, J., Vila, F., Sarró, S., Capdevila, A., Bullmore, E., 2008. A simple view of the brain through a frequency-specific functional connectivity measure. Neuroimage 39, 279–289.
Salvador, R., Suckling, J., Schwarzbauer, C., Bullmore, E., 2005. Undirected graphs of frequency-dependent functional connectivity in whole brain networks. Philos. Trans. R. Soc. Lond. B Biol. Sci. 360, 937–946.
Schmidt, M.F., Ashmore, R.C., Vu, E.T., 2006. Bilateral control and interhemispheric coordination in the avian song motor system. Ann. N. Y. Acad. Sci. 1016, 171–186.
Shen, J., 2014. Tools for NIfTI and ANALYZE Image.
Shen, K., Mišić, B., Cipollini, B.N., Bezgin, G., Buschkuehl, M., Hutchison, R.M., Jaeggi, S.M., Kross, E., Peltier, S.J., Everling, S., 2015. Stable long-range interhemispheric coordination is supported by direct anatomical projections. Proc. Natl. Acad. Sci. Unit. States Am. 112, 6473–6478.
Shtoyerman, E., Arieli, A., Slovin, H., Vanzetta, I., Grinvald, A., 2000. Long-term optical imaging and spectroscopy reveal mechanisms underlying the intrinsic signal and stability of cortical maps in V1 of behaving monkeys. J. Neurosci. 20, 8111–8121.
Sladky, R., Friston, K.J., Tröstl, J., Cunnington, R., Moser, E., Windischberger, C., 2011. Slice-timing effects and their correction in functional MRI. Neuroimage 58, 588–594.
Sperry, R.W., 1968. Plasticity of neural maturation. Dev. Biol. 2, 306–327.
Stark, D.E., Margulies, D.S., Shehzad, Z.E., Reiss, P., Kelly, A.C., Uddin, L.Q., Gee, D.G., Roy, A.K., Banich, M.T., Castellanos, F.X., 2008. Regional variation in interhemispheric coordination of intrinsic hemodynamic fluctuations. J. Neurosci. 28, 13754–13764.
Striedter, G.F., Vu, E.T., 1998. Bilateral feedback projections to the forebrain in the premotor network for singing in zebra finches. Dev. Neurobiol. 34, 27–40.
Tadel, F., Baillet, S., Mosher, J.C., Pantazis, D., Leahy, R.M., 2011. Brainstorm: a user-friendly application for MEG/EEG analysis. Intell. Neurosci. 8 (1–8), 13, 2011.
Tanabe, J., Miller, D., Tregellas, J., Freedman, R., Meyer, F.G., 2002. Comparison of detrending methods for optimal fMRI preprocessing. Neuroimage 15, 902–907.
Toulmin, H., Beckmann, C.F., O'Muircheartaigh, J., Ball, G., Nongena, P., Makropoulos, A., Ederies, A., Counsell, S.J., Kennea, N., Arichi, T., Tusor, N., Rutherford, M.A., Azzopardi, D., Gonzalez-Cinca, N., Hajnal, J.V., Edwards, A.D., 2015. Specialization and integration of functional thalamocortical connectivity in the human infant. Proc. Natl. Acad. Sci. Unit. States Am. 112, 6485–6490.
Tovar-Moll, F., Monteiro, M., Andrade, J., Bramati, I.E., Vianna-Barbosa, R., Marins, T., Rodrigues, E., Dantas, N., Behrens, T.E., de Oliveira-Souza, R., 2014. Structural and functional brain rewiring clarifies preserved interhemispheric transfer in humans born without the corpus callosum. Proc. Natl. Acad. Sci. Unit. States Am. 111, 7843–7848.
Triantafyllou, C., Hoge, R.D., Krueger, G., Wiggins, C.J., Potthast, A., Wiggins, G.C., Wald, L.L., 2005. Comparison of physiological noise at 1.5 T, 3 T and 7 T and optimization of fMRI acquisition parameters. Neuroimage 26, 243–250.
Turchi, J., Chang, C., Ye, F.Q., Russ, B.E., Yu, D.K., Cortes, C.R., Monosov, I.E., Duyn, J.H., Leopold, D.A., 2018. The basal forebrain regulates global resting-state fMRI fluctuations. Neuron 97, 940–952 e4.
Tustison, N.J., Avants, B.B., Cook, P.A., Zheng, Y., Egan, A., Yushkevich, P.A., Gee, J.C., 2010. N4ITK: improved N3 bias correction. IEEE Trans. Med. Imaging 29, 1310–1320.
Tyszka, J.M., Kennedy, D.P., Adolphs, R., Paul, L.K., 2011. Intact bilateral resting-state networks in the absence of the corpus callosum. J. Neurosci. 31, 15154–15162.
Uddin, L.Q., Mooshagian, E., Zaidel, E., Scheres, A., Margulies, D.S., Kelly, A.M.C., Shehzad, Z., Adelstein, J.S., Castellanos, F.X., Biswal, B.B., Milham, M.P., 2008. Residual functional connectivity in the split-brain revealed with resting-state fMRI. Neuroreport 19, 703–709.
van der Knaap, L.J., van der Ham, I.J., 2011. How does the corpus callosum mediate interhemispheric transfer? A review. Behav. Brain Res. 223, 211–221.
Van Essen, D.C., 2005. Corticocortical and thalamocortical information flow in the primate visual system. In: Progress in Brain Research. Cortical Function: a View from the Thalamus. Elsevier, pp. 173–185.
Van Meir, V., Boumans, T., De Groof, G., Van Audekerke, J., Smolders, A., Scheunders, P., Sijbers, J., Verhoye, M., Balthazart, J., Van der Linden, A., 2005. Spatiotemporal properties of the BOLD response in the songbirds' auditory circuit during a variety of listening tasks. Neuroimage 25, 1242–1255.
Van Ruijssevelt, L., Hamaide, J., Van Gurp, M.T., Verhoye, M., Van der Linden, A., 2017. Auditory evoked BOLD responses in awake compared to lightly anaesthetized zebra finches. Sci. Rep. 7 (1), 13563.
Van Ruijssevelt, L., Van der Kant, A., De Groof, G., Van der Linden, A., 2013. Current state-of-the-art of auditory functional MRI (fMRI) on zebra finches: Technique and scientific achievements. J. Physiol. Paris 1073), 156–169.
Vates, G.E., Broome, B.M., Mello, C.V., Nottebohm, F., 1996. Auditory pathways of caudal telencephalon and their relation to the song system of adult male zebra finches (Taenopygia guttata). J. Comp. Neurol. 366, 613–642.
Vincent, J.L., Patel, G.H., Fox, M.D., Snyder, A.Z., Baker, J.T., Essen, D.C.V., Zempel, J.M., Snyder, L.H., Corbetta, M., Raichle, M.E., 2007. Intrinsic functional architecture in the anaesthetized monkey brain. Nature 447, 83–86.
Wang, J., Wang, L., Zang, Y., Yang, H., Tang, H., Gong, Q., Chen, Z., Zhu, C., He, Y., 2009. Parcellation-dependent small-world brain functional networks: a resting-state fMRI study. Hum. Brain Mapp. 30, 1511–1523.
Welvaert, M., Rosseel, Y., 2013. On the definition of signal-to-noise ratio and contrast-to-noise ratio for fMRI data. PLoS One 8, e77089.
Whitfield-Gabrieli, S., Nieto-Castanon, A., 2012. Conn: a functional connectivity toolbox for correlated and anticorrelated brain networks. Brain Connect. 2, 125–141.
Wild, J.M., Li, D., Eagleton, C., 1997. Projections of the dorsomedial nucleus of the intercollicular complex (DM) in relation to respiratory-vocal nuclei in the brainstem of pigeon (Columba livia) and zebra finch (Taeniopygia guttata). J. Comp. Neurol. 377, 392–413.
Wild, J.M., Williams, M.N., Suthers, R.A., 2000. Neural pathways for bilateral vocal control in songbirds. J. Comp. Neurol. 423, 413–426.
Yan, C.-G., Wang, X.-D., Zuo, X.-N., Zang, Y.-F., 2016. DPABI: data processing & analysis for (resting-state) brain imaging. Neuroinformatics 14, 339–351.

Yoshida, K., Mimura, Y., Ishihara, R., Nishida, H., Komaki, Y., Minakuchi, T., Tsurugizawa, T., Mimura, M., Okano, H., Tanaka, K.F., Takata, N., 2016. Physiological effects of a habituation procedure for functional MRI in awake mice using a cryogenic radiofrequency probe. J. Neurosci. Methods 274, 38–48.
Zhang, J., Kendrick, K.M., Lu, G., Feng, J., 2014. The fault lies on the other side: altered brain functional connectivity in psychiatric disorders is mainly caused by counterpart regions in the opposite hemisphere. Cerebr. Cortex 25, 3475–3486.
Zhao, F., Jin, T., Wang, P., Kim, S.-G., 2007. Isoflurane anesthesia effect in functional imaging studies. Neuroimage 38, 3.
Zhou, Y., Milham, M., Zuo, X.-N., Kelly, C., Jaggi, H., Herbert, J., Grossman, R.I., Ge, Y., 2013. Functional homotopic changes in multiple sclerosis with resting-state functional MR imaging. Am. J. Neuroradiol. 34, 1180–1187.
Zuo, X.-N., Kelly, C., Di Martino, A., Mennes, M., Margulies, D.S., Bangaru, S., Grzadzinski, R., Evans, A.C., Zang, Y.-F., Castellanos, F.X., 2010. Growing together and growing apart: regional and sex differences in the lifespan developmental trajectories of functional homotopy. J. Neurosci. 30, 15034–15043.
Zwaag, W van der, Marques, J.P., Kober, T., Glover, G., Gruetter, R., Krueger, G., 2012. Temporal SNR characteristics in segmented 3D-EPI at 7T. Magn. Reson. Med. 67, 344–352.